3151

Research Report

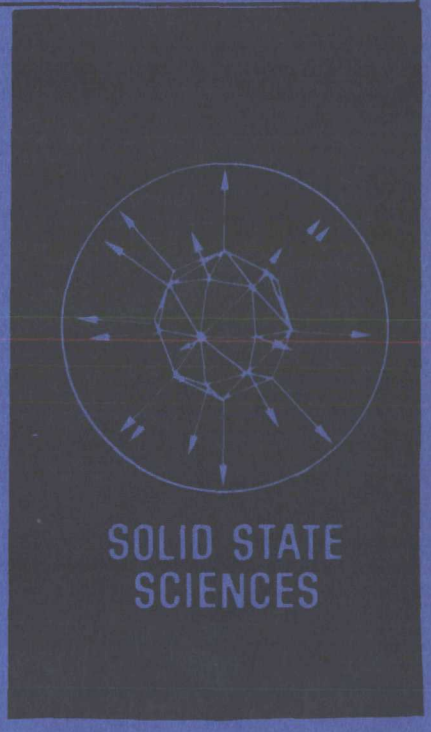

SC-RR-72 0814
December 1972

SHOCK RESPONSE OF DISTENDED CVD CARBON FELT

L. M. Lee
Shock Wave Physics Division 5133

SANDIA LABORATORIES

OPERATED FOR THE UNITED STATES ATOMIC ENERGY COMMISSION BY SANDIA CORPORATION | ALBUQUERQUE, NEW MEXICO LIVERMORE, CALIFORNIA

DISCLAIMER

Issued by Sandia Laboratories,
a prime contractor to the
United States Atomic Energy Commission

Printed in the United States of America

Available from:
National Technical Information Service
U. S. Department of Commerce
5285 Port Royal Road
Springfield, Virginia 22151
Price: Printed Copy $3.00; Microfiche $0.95

December 1972

SC-RR-72 0814

SHOCK RESPONSE OF DISTENDED CVD CARBON FELT

L. M. Lee

Sandia Laboratories, Albuquerque, New Mexico 87115

Abstract

A study directed at determining the stress-wave propagation behavior in distended CVD carbon felt heat shield material is described and the results presented. The primary objective was to experimentally investigate the shock response of the porous carbon felt and provide information defining the material's dynamic mechanical equation-of-state. The results from the shock experiments included Hugoniot and release adiabat data, attenuated wave profile measurements, and spallation data. The equation-of-state parameters necessary for shock attenuation calculations were provided by the Hugoniot and release data, making possible a critical comparison between the experimentally measured and calculated shock attenuation response. The calculated response was in good agreement with the attenuation data, both in wave shape and amplitude. Static confined compression experiments were conducted, in conjunction with ultrasonic measurements at load, to provide sound speed data during unloading. These data showed a marked variation in release velocity as a function of compaction state. The static samples were also evaluated for internal damage resulting from compression. The material damage was found to be minimal and localized to material surrounding the pores.

ACKNOWLEDGMENT

The author is indebted to L. A. Kent, C. L. Witten and G. E. Ingram for their contributions in the experimental program and to J. K. Johnstone for making the results of his SEM study available.

I. INTRODUCTION

Sandia designed reentry vehicles have made use of chemical vapor deposited (CVD) carbon felt heatshields. CVD felt heatshields have been successfully flight tested and the material is a candidate for advanced reentry applications. In view of the general interest in carbon felt, a material evaluation program has been conducted to characterize certain physical and mechanical properties of the specific felt used in these heatshields. Both dynamic structural tests and underground experiments in Nevada are included in this program. Analysis of these experiments, as well as advanced systems design, is dependent on proper characterization of the CVD carbon felt's stress wave propagation behavior. The primary purpose of the study reported here was to experimentally investigate the shock response of the porous felt and provide information defining the material's dynamic mechanical equation-of-state. The current carbon felt experimental results have also been compared with data on other similar carbon materials, to provide a more comprehensive view of porous carbon shock behavior.

The CVD felt investigated was designated flight material because the test specimens were taken from a candidate heatshield, rather than from flat plates. Even though there are only slight differences in the manufacturing techniques used to produce flat plates and conical shapes of carbon felt, parts produced by the two different manufacturing techniques have shown marked differences in their static mechanical properties. The heatshield material used in this study was processed by means of a low pressure isothermal method, which resulted in a carbon matrix substantially different from the felts that have been previously investigated.

The experimental portion of the study provided all of the equation-of-state information required for numerical shock attenuation calculations in the distended CVD felt. The dynamic measurements included Hugoniot and release adiabat data, attenuated stress profiles after propagation through various thicknesses of material, and spallation information. The material parameters necessary to make shock attenuation calculations in the porous carbon felt were completely defined by the Hugoniot and release adiabat data, thus making possible a critical comparison between predicted and measured attenuation responses. The calculated responses were in good agreement with the attenuation experiments, both in pulse amplitude and wave shape, over the propagation distances investigated (2.0 to 6.4 mm). Significant attenuation and spreading of the stress pulse was observed in these experiments.

Static confined compression experiments were conducted, in addition to the shock experiments, to obtain complete one-dimensional strain loading and unloading response for comparison with the dynamic results. Ultrasonic velocity measurements were made during the tests to evaluate the variation in sound speed during the loading and unloading cycles. Both the ultrasonic data and the sound speeds calculated from the static stress-strain curves showed a marked variation in the initial velocity of an unloading wave as a function of the compaction state. The release wave speeds determined statically were in general agreement with the shock data. The post test static compression specimens were also evaluated for internal material damage using ultrasonic and scanning electron microscope techniques.

The spallation results showed that the flight quality CVD felt had a higher resistance to spallation than almost all carbon materials previously studied. The increased spall resistance, in conjunction with the highly attenuative

behavior of the CVD felt, makes it a very desirable heatshield material from a shock response standpoint.

II. MATERIAL DESCRIPTION AND CHARACTERIZATION

The carbon felt specimens used in this study were taken from a conical heatshield (designation STC-6) produced by a chemical vapor deposition (CVD) process. The material fabrication process started with a needled rayon felt formed into a conical shape. The rayon felt was then carbonized to produce a carbon felt with an approximate density of 0.1 g/cm^3. The carbon felt was then densified with CVD pyrolytic carbon. The CVD process depends upon the thermal decomposition of hydrocarbon gases and the formation of pyrolytic carbon on the surfaces of the carbon felt fibers. The densification was carried out at a temperature of 1100°C and a pressure of 10-30 torr until the desired final density was achieved. The cone was subsequently heat treated at 2750°C for 2 hours as a final graphitization cycle. A complete description of the fabrication process can be found in Ref. 1.

Proper characterization of the CVD carbon felt was necessary if meaningful correlations between the shock response of this material and other porous carbon systems were to be made. The structural form of the carbon present in the CVD felt was one important characteristic that was investigated. Carbon can exist in a wide range of crystallographic forms, with a corresponding wide variation in material properties. This is illustrated by a comparison of diamond, one of the hardest materials known, to graphite, one of the softest. This wide range of possible polymorphic forms and physical properties made it imperative to evaluate the crystalline state of the carbon present in the CVD felt. The crystalline form of carbon in the CVD felt was determined from x-ray diffraction measurements. The d_{002} interplanar spacing was found to be 3.362Å, as compared to 3.35Å for hexagonal

single crystal graphite.[2,3] The apparent crystallite sizes were calculated from line broadening and found to be 300Å (L_c) in the c crystallographic direction and 259Å (L_a) in the ab plane.[2] These crystallographic parameters indicated that the CVD carbon felt was highly graphitic.

The porosity present in the CVD felt was another important material characteristic that was evaluated. The type and uniformity of the pores in the carbon felt were examined both optically and with a scanning electron microscope (SEM). The pores were uniformly distributed, with the bulk of the distention resulting from roughly equidimensional voids ranging in size from 20 to 250 microns. The type of porosity present in the CVD felt is shown in the typical photomicrographs from the SEM work in Figure 1.[4] The pores in the photomicrograph are the dark areas outlined with white borders. The white borders are edge effects caused by electron scattering at the edge of the pores. The dark spots and lines in Figure 1 represent the carbonized felt, with the grey region being the CVD pyrolytic carbon. The photomicrographs also indicated that the total distention consisted of both open and closed pores.

The density of the solid material in the CVD carbon felt was also investigated. Knowledge of the average solid material density of the felt was necessary in modeling the shock compaction behavior of the porous material. However, the closed porosity in the CVD felt made a direct pycnometry measurement of the solid material density questionable. Helium pycnometer measurements were nevertheless made on a number of test specimens and yielded an average solid material density of 1.98 g/cm^3.[4] This density value was taken as a lower bound on the solid material because of the closed porosity. Pycnometry measurements were also made on the same samples after they had been statically compressed to 5.0 kbars. It was anticipated that the loading would create some internal cracking and open a portion of the closed pores to the helium. The results on the compressed samples gave an

average density of 2.02 g/cm^3. Post compression SEM work, however, revealed a degree of residual closed porosity which still influenced the density measurement.

The second approach used to determine the solid density made use of the known volume fractions[4] of carbonized felt and pyrolytic carbon in the material and considered them as a simple mixture. Based on a 7% fiber volume, the calculated solid material density was 2.17 g/cm^3. This value was not influenced by the closed porosity and was used as the solid constituent density in the modeling calculations.

The average density of the CVD carbon felt specimens used in this study was 1.73 g/cm^3. The samples contained on the average 20% total porosity, with the closed porosity being approximately 7%, based on a solid material density of 2.17 g/cm^3.

III. EXPERIMENTAL TECHNIQUES

Shock Compaction and Release Experiments

The shock response of the CVD carbon felt was studied under conditions of uniaxial strain shock loading. Stress pulses were produced either by using a gas gun to impact a flat plate into the specimen, or by explosive loading. Various experimental configurations and instrumentation were used to obtain the Hugoniot and release adiabat data, attenuated stress wave profiles, and spallation data. The data analysis employed the Rankine-Hugoniot[5] jump equations, which assume steady wave behavior and thermodynamic equilibrium behind the shock front. The applicability of these equations to describe the shock propagation behavior of the CVD felt was investigated.

The shock loading and release characteristics below 30 kbars were obtained from three different types of plate-impact experiments performed with a gas gun.[6] The first was a buffer plate experiment, designed to provide a stress

(σ_x)-particle velocity (u_p) Hugoniot point. In this experiment, a CVD carbon felt sample impacted an elastic buffer plate, with the resulting stress pulse propagating through the buffer plate and interacting with an X-cut quartz gauge[7] mounted on the rear surface of the plate. The measured quantities included impact velocity and the time resolved current output of the quartz gauge as measured by the voltage across a 50-ohm termination resistor. Three different buffer plate materials with known shock wave properties were used in the experiments: fused silica,[8] 4340 R_c 54 steel,[9] and tungsten carbide.[10] Elastic impedance-match calculations were made at the buffer-quartz interface to determine the (σ_x, u_p) state in the buffer prior to the stress wave interaction with the quartz. The boundary conditions of stress and particle velocity continuity across the felt-buffer plate interface at impact were then used to calculate the (σ_x, u_p) state for the CVD felt.

The second type of experiment, which furnished both Hugoniot and release adiabat data, made use of shock-reverberation techniques.[11] Two experimental configurations, shown schematically in Figures 2 and 3, were employed. One consisted of a thin quartz gauge as the reverberation plate (Figure 2) and the other a thin 4340 R_c 54 steel reverberation disk, in conjunction with a displacement interferometer.[12] Figure 2a depicts the experimental configuration for the quartz crystal assembly and 3a the assembly for the interferometer system. Figures 2b and 3b illustrate the shock response of each material component in the stress-particle velocity plane. A carbon felt sample was mounted on a projectile nose and impacted into a reverberation plate to generate the stress pulse. The thicknesses of the carbon sample and reverberation plate were such that the wave could reverberate a number of times in the plate without being influenced by side or rear rarefaction waves. The initial shock state established on impact is point (1) in Figures 2b and 3b and states on the carbon release

adiabat are designated as points (3) and (5). The stress levels at points (1), (3) and (5) were measured directly when a quartz gauge reverberation plate was used (Figure 2b). Free surface velocity data were recorded when the steel reverberation plate was employed (Figure 3b, points (2), (4) and (6)). Elastic impedance calculations were used, in conjunction with the steel free surface velocity data, to determine the stress-particle velocity states in the carbon. Because of the relative mechanical impedances of the materials, it was difficult to obtain more than one or two points on a single carbon release adiabat per experiment.

The buffer-plate and reverberating wave experiments provided shock compaction and release adiabat data directly, but did not provide sufficient information to define the path followed by the felt in loading to an equilibrium state. However, the loading path can be deduced from the structure of a transmitted stress pulse. Consequently the third basic type of plate impact experiment performed on the CVD felt was a transmitted-wave experiment so that the structure of transmitted stress pulses could be observed. A double quartz gauge technique, similar to that described by Halpin, et. al.,[13] was used to measure the stress input into the carbon sample and the resulting transmitted wave profile. The experimental assembly is shown in Figure 4. A 4340 R_c 54 steel plate with a quartz crystal mounted on the rear surface was the impactor in this configuration. The steel made it possible to achieve impact over the entire area of the large diameter carbon sample, which was necessary to eliminate edge rarefactions. The target was the CVD felt sample backed by another quartz gauge. Data on the impact stress and the transmitted wave shape were thus obtained from a single experiment. The impact time and tilt were obtained from flush-pin records[6] and were used, in conjunction with the target gauge, to determine the stress pulse transit time through the sample. The transit time measurement made it possible to calculate

an average compaction wave velocity through the sample. The impact state parameters, (σ_x, u_p), measured by the projectile gauge were then directly compared with the calculated impact conditions arrived at by use of the Hugoniot equations and the compaction wave speed. General agreement was found between the measured and calculated compaction state parameters for the carbon felt.

The dynamic compaction behavior of the carbons above 30 kbars was characterized by the use of standard explosive techniques.[5] A carbon specimen and a specimen of copper, which has a well-documented equation of state,[14] were placed on a standard-material driver plate that was in direct contact with various explosive assemblies. Figure 5 is a schematic of the test assembly. A quartz gauge was mounted on the rear surface of the carbon specimen and quartz shorting pins were placed on the driver plate and on the standard copper specimen. Shock transit times through the carbon and standard specimens were thus obtained and average shock velocities were calculated. The quartz gauge also provided data on the shock profile transmitted through the carbon. In all the explosive experiments a single wave was recorded by the quartz. The Hugoniot data were determined using the impedance-matching techniques described by Rice, et. al.[5]

Attenuation Measurements

Attenuated-wave profile measurements were made on the porous CVD carbon, to obtain an independent set of experimental data for direct comparison with calculated attenuation response. These data were obtained from gas-gun experiments in which thin impactors were used to generate the input stress pulses. The impact velocity was held constant and only the target thickness was varied. The data consisted of measured attenuated stress-time profiles as a function of propagation distance through the carbon felt.

Figure 6 shows the attenuation experiment configuration. The projectile consisted of a thin fused silica impactor plate, nominally 1.7 mm thick, backed by a very low-density carbon foam with known dynamic mechanical properties.[15] The impact stresses were below the elastic limit of the impactor material, thus simplifying calculation of the stress-wave shape introduced into the samples. Also, the relatively high elastic-wave speed of the fused silica permitted the generation of reasonably short-duration stress pulses without recourse to excessively thin impactors.

The target design for the attenuation shots was essentially the same as for the transmitted-wave experiments. Carbon sample thicknesses ranging from 2.0 to 6.4 mm were used to give the desired variation in propagation distance. Impact velocity and tilt were measured as previously described. The attenuated stress pulses were recorded with manganin back surface gauges because of the need for long recording times, as well as a desire for a back surface gauge that closely matched the mechanical impedance of the carbon. A commercially available four-terminal manganin wire (.076 mm diameter) in C-7 epoxy transducer was used.[16,17,18] In the course of the investigation calibration experiments were conducted to define the change in resistance of the gauges as a function of applied stress. This calibration data made it possible to convert the manganin voltage-time records to stress-time records in the C-7 epoxy. The results of the attenuation experiments were then plotted in the stress-time plane, with impact being the zero-time reference common to all data. These data clearly showed the degree of attenuation as a function of propagation distance through the CVD felt. The profiles were also compared with the calculated material response by using the previously generated carbon equation-of-state parameters and a porous material model.

Confined Static Compression and Release

Static laterally constrained compression experiments were also conducted in this investigation to obtain static one-dimensional strain data for comparison with the dynamic results. The static experiments provided complete loading and unloading curves, in addition to qualitative information on fracturing in the porous carbons during compression. Ultrasonic velocity measurements made during the load cycle were also used to determine sound velocities in the material during unloading. The experimental configuration used to simulate the one-dimensional strain condition, shown in Figure 7, is similar to a previously used technique.[19] The carbon sample was placed in the cylinder and the two load rams were inserted as shown. Next the assembly was placed between the platens of the test machine (Material Test System Model 810), and the displacement-measuring transducer installed. The specimen was then loaded and unloaded at a rate of .05 cm/min., with piston load and displacement being monitored. Maximum load was 5.1 kbars. At specific points during the load-release cycle transit time measurements of an ultrasonic pulse were made through the load rams and sample. A pulse transmission technique, employing 1 MHz barium titanate transducers, was used for these measurements.[20] The transit time through the sample was determined by subtracting the propagation time through the rams from the total measured pulse transit time. The propagation time through the rams was measured on a previous calibration run in which no sample was used. Also, the calibration run provided load-displacement data for the rams alone, which was used to correct the sample traces for the elastic deformation of the loading rams.

The confined compression experiment was designed to approximate a static one-dimensional strain condition with the principal strain in the axial direction. Two factors in this type of experiment make it difficult to achieve a uniform

one-dimensional strain state in the sample. They are (1) radial expansion of the confining cylinder and (2) frictional effects along the walls of the confining cylinder. The first allows lateral deformation of the sample, which compromises the one-dimensionality of the strain. However, the maximum radial strain at the inner diameter of the confining cylinder was only about 0.2 percent, based on elasticity calculations at maximum load. Compared to the axial strain of the porous CVD felt (up to 20 percent at maximum load), radial cylinder expansion was considered a second-order effect. The second compromising factor, frictional effects, was also evaluated. If frictional forces against the constraining cylinder become large enough, appreciable stress and strain gradients can be produced in the sample. The lateral frictional forces were measured during the compression tests and found to be minimal. The worst condition occurred at maximum load, where the frictional load was 2.2% of the axial load. Based on these observations it was concluded that the static confined compression experiment produced essentially a one-dimensional strain state in the CVD felt. Ultrasonic velocity measurements were also made on most of the specimens used in the shock experiments. These measurements were made using the pulse transmission technique. PZT crystals were used for the longitudinal wave speeds and AC cut quartz crystals for the shear-wave measurements.

Spallation Experiments

A series of experiments was conducted to characterize the spallation resistance of the CVD carbon felt. The gas gun was used to launch a carbon felt impactor against a felt target, as shown in Figure 8. The target was a tapered plug mounted in an aluminum target plate. The carbon felt was potted in the target ring with a very viscous epoxy to minimize penetration into pores. Mold release was put on the aluminum plate so that the target plug could easily

be separated from the plate upon impact. As illustrated in Figure 8, both the CVD felt impactor and target had free rear surfaces. Wave reflections from these surfaces caused the production of rarefaction waves which interacted in the target to produce a tensile pulse. The target plugs were recovered in a soft recovery system (the stripper cone is shown in Figure 8) that prevented secondary impacts and allowed for slow deceleration of the specimen. The impact velocity of the projectile was measured and damage, if any, was observed by sectioning the target plug. Two different target thicknesses were investigated (nominally 7.62 mm and 3.81 mm), with the impactor in each experiment having a thickness equal to one half the target thickness.

IV. EXPERIMENTAL RESULTS AND ANALYSIS

Shock Compression and Release Behavior

The impact experiments provided a variety of information on the shock compaction and release behavior of the CVD carbon felt. Records from typical buffer-plate and reverberating-wave experiments are shown in Figure 9. The results of a transmitted-wave experiment using the double quartz gauge technique are given in Figure 10. It can be seen from both Figures 9 and 10 that there were no measurable initial transient overshoots in stress at the impact surface and stress equilibrium was achieved very rapidly. These data indicate apparent rate insensitive response for the CVD carbon felt. The transmitted-wave profile in Figure 10b shows a very low amplitude ramp wave preceding the main compaction wave. This type of response was observed on all of the low stress transmitted wave experiments. The shape and amplitude of the ramp precursor were interpreted as indicating a very low-strength, non-linear compressional yield region in the felt prior to major void compaction. However, when the compaction wave amplitude was 10 kbar or larger, the precursor was completely overdriven. The average

precursor breakaway velocity of 2.47 mm/μsec was difficult to determine because of the ramp wave shape. This value compares favorably with the average ultrasonically measured longitudinal wave speed of 2.67 mm/μsec. The average half-amplitude precursor velocity was 1.73 mm/μsec. Similar yield behavior was also observed in the static, laterally confined compression tests.

The results of the shock compaction experiments are given in Table I along with the initial sample conditions and the type of experiment used to generate the data. The applicability of the Hugoniot relations to describe the wave propagation behavior in the carbon felt was evaluated from the transmitted wave data listed in Table I. A direct comparison was made between the shock wave velocity (U), measured in each transmitted wave experiment, and the calculated shock speed. The calculated value of U was evaluated by using the impact state conditions and the Hugoniot equations. The good agreement between the measured and calculated shock velocity data attests to the applicability of the jump conditions.

All of the Hugoniot data are plotted in Figure 11. Also shown in Figure 11 is the Hugoniot for solid graphite[21] centered at an initial density of 2.17 g/cm^3. The fair agreement between the high stress data (above 10 kbar) and the solid graphite response indicates that the fully compacted felt can be modeled using the graphite Hugoniot. The data scatter in the stress-specific volume plane was attributed primarily to sample variations in initial density (densities ranged from 1.69 to 1.80 g/cm^3).

The lower stress Hugoniot data are plotted on an expanded scale in Figure 12 to show more clearly the partially compacted region. A calculated partial compaction curve using the P-α representation[22] is also shown in Figure 12. This curve represents the compaction data reasonably well. The parameters used to describe the CVD felt and solid graphite in the model are listed in Table II.

It can be seen from Figure 12 that the CVD felt compacts to a no-void condition at a relatively low stress level. Compaction behavior of this type is more characteristic of porous graphites (ATJ and LASL), than previously studied carbon-carbon composites.[21,23,24] An important point to remember is that the P-α model defines the distended material response as linearly elastic prior to yielding. As previously established by the transmitted-wave profiles and static data, the observed yield region was not linear but very rounded, causing spreading of the precursor wave. Because of this spreading, the half-amplitude precursor wave speed was used in the model, rather than the breakaway velocity.

The release adiabat data determined from the shock reverberation experiments are also shown in Figure 12. The data associated with a single experiment are shown connected by a straight line. As previously mentioned, only one or two points on a single release path were measured per experiment. In view of the limited data, release paths were assumed to be straight lines connecting the shock and release states. An average release wave velocity was calculated from the slope of these lines by applying the jump conditions between the Hugoniot states and release states. The velocities are denoted $\overline{U}_R$. The release adiabat data are listed in Table I.

Characterizing the unloading response of the CVD felt as strictly linear was obviously an oversimplification based on the static confined compression and release data. However, two important features of the release wave response were evident from the release adiabat data. First, the release states were considerably offset from the Hugoniot, which resulted in fast release wave speeds relative to compaction wave velocities. Secondly, the linear unloading paths became steeper as the Hugoniot stress was increased. Both of these factors work to increase the degree of stress wave attenuation in the carbon felt.

Attenuation Data

The attenuated stress wave profile measurements provided information on the wave amplitude, shape, and shock transit time through the samples. The fused silica impactor produced an input stress pulse that was an initial step at impact to the maximum stress level, followed by a ringing down in stress resulting from wave reverberations in the thin impactor. The time associated with each step in the ring down process was approximately 0.56 μsec. Records from the four attenuation shots are shown in Figure 13 and the experimental conditions for these shots are summarized in Table III. Figure 13 shows some spreading of the compaction wave as a function of propagation distance. The release segments of the attenuated wave profiles from the 2.0 mm thick targets have a somewhat stair-step appearance, reflecting the discrete unloading steps associated with the impactor ring down. The discrete steps were completely smoothed out, however, after propagation through 4.0 mm of the CVD felt.

The experimental voltage-time records were digitized and converted to stress-time data in the manganin gauge. Zero time represents impact. The reduced attenuated wave data are plotted together in Figure 14 to illustrate the change in wave shape and amplitude with propagation distance. Also shown in Figure 14 are the predicted attenuated wave profiles, calculated using the WONDY IV wave propagation code[25] and the experimental impact conditions. The equation-of-state parameters (Table II) determined from the shock compaction and release data were used in the code to model the CVD felt. The good overall agreement between the calculated and measured attenuated wave shapes verifies that the porous material equation-of-state and model adequately represent the CVD felt mechanical wave-propagation behavior. Another check on the correlation calculations was provided by comparing the calculated impact stress with the impact stress

measured on three identical, independent experiments. The measured impact stress was from 15 to 16 kbar, which correlated well with the 15.5 kbar calculated by the code.

Static Confined Compression Results

The static, laterally confined compression tests provided data on both the loading and release characteristics of the CVD carbon felt and information on internal material damage resulting from compression. The static, one dimensional strain response was determined from the load-deflection curves and ultrasonic measurements. The extent of material damage resulting from static compression was qualitatively investigated by ultrasonic and SEM techniques.

Representative static stress-specific volume plots for the CVD carbon are shown in Figure 15. The low stress, shock compaction data and the solid graphite Hugoniot are included in Figure 15a for comparison. Fair quantitative agreement was obtained between the static and dynamic data in the partially compacted region. The offset between the static compaction curve and solid graphite Hugoniot at 5.0 kbar was attributed to experimental scatter and was not considered significant. The general agreement between the shock and static results was felt to indicate a lack of rate sensitivity in the felt. Also correlation between the two types of data illustrates that the static technique may be used to estimate the shock compaction response for rate insensitive porous carbon materials.

The primary purpose for conducting the static experiments was to obtain complete unloading paths for the carbon felt. These paths could not be determined in the shock experiments for reasons previously discussed. The static unloading response of the carbon felt is shown in Figures 15. Figure 15a shows a single load-release curve and 15b and c show multiple loading and unloading cycles.

The unloading paths were initially steep and reasonably linear until unloading stresses of about 0.5 kbar was reached. After this the unloading became quite nonlinear and showed a high degree of void recovery when the static compression was removed. Residual strains in the material after unloading were on the order of 4 to 5% while maximum compressional strains of 18 to 19% were experienced during the tests. All the compression samples were intact after testing, with no external evidence of material damage. It was concluded from these results that the low stress void recovery exhibited by the carbon felt was the product of a large non-linear elastic strain component associated with the static compaction.

The measured static unloading paths provided quantitative information on the release behavior of the CVD felt, in addition to qualitative information on void recovery. The quantitative information consisted of sound speed data associated with the different static release paths. These wave velocities were calculated from the stress-specific volume data using the relation:

$$C_{1-2} = v_1\left(\frac{\sigma_1 - \sigma_2}{v_2 - v_1}\right)^{1/2}$$

where C_{1-2} is the velocity associated with the release wave increment 1-2. Release wave velocities, determined from the initial 0.1 kbar stress increment of the unloading paths, were calculated to investigate the variation in initial release wave speed with compaction state. Also these initial release wave speeds were measured ultrasonically during the static test, thus providing an independent set of data to compare with the calculated velocities. The results of the ultrasonic measurements and static calculations are shown in Figure 16. The two sets of initial release wave speed data are in good agreement,

indicating that the confined compression test does provide an accurate representation of the distended carbon's initial unloading behavior.

A second comparison of release velocity data was made and is included in Figure 16. This comparison was between the average C_{1-2} release wave velocities determined from the shock reverberation experiments and the corresponding velocities calculated from the static stress-strain data. The same magnitude stress increment that was measured in the shock release experiment was used in the corresponding calculation with the static data. Agreement between the average wave speed data was felt to further verify the applicability of the static test technique to determine the porous carbon felt response. The data in Figure 16 clearly show the variation in release wave speed as a function of compaction state. The different magnitudes of the initial and average velocities for a given compaction stress are a result of the curvature in the unloading path.

Qualitative information on internal material damage due to compression loading was obtained through ultrasonic and SEM work. The ultrasonic measurements consisted of longitudinal velocities measured before and after the static tests. A decrease in the post-test ultrasonic velocities was observed, which was attributed to internal fractures in the carbon felt created by the load cycle. The velocities continued to decrease as the number of loading cycles increased although the same maximum load was reached in all the tests. The numerical results of the ultrasonic measurements are summarized in Table IV.

The SEM investigation of the static test samples provided more explicit information on the internal material damage.[4] The post-test pore structure was qualitatively the same as the pre-test material, with evidence of only localized internal damage. The damage was confined to the material surrounding the pores and did not extend into the solid bulk material. Usually the fracturing was limited to only one or two of the fiber-pyrocarbon cylinders that surrounded

the pore, with the remainder of the material appearing to retain its original integrity. Figures 17 and 18 contain photomicrographs that illustrate the type of damage that was observed. The b and c portions of each figure are enlargements of the central region of the a photomicrograph. The samples in Figure 17 and 18 experienced a single load cycle to 5.1 kbars and were then unloaded. Figure 17c shows one of the pyrocarbon shells that fractured during loading. It appears that the carbon failed in shear as the pore was closed, but then returned to basically its original position upon load removal. The other pyrocarbon surrounding the pore appears to have deformed in a completely elastic manner. Figure 18 illustrates damage to the pyrocarbon of a more drastic nature. The pore structure in this region was of a finer nature, producing more unsupported felt fiber-pyrocarbon cylinders. However, the fracturing evidenced in Figure 18 was still on a local scale with only a small percentage of the material damaged. Based on the SEM work, it was concluded that only minimal internal material damage resulted from effectively total pore closure.

Spallation Results

The objective of the spallation experiments was to measure the impact velocities that produced incipient and complete spall in the CVD felt targets. Symmetric impact conditions with a target-to-impactor thickness ratio of two were used so that the current data would be directly comparable with spall data on other distended carbons. The experimental spall data generated on the felt are summarized in Table V. The experimental details and the observed degree of fracture upon sectioning the targets are included in Table V. Incipient spall was defined as the formation of cracks in the midplane of the target that were observable under low power magnification (0-20X). The impact velocities necessary to create incipient spall were .08 mm/μsec and .11 mm/μsec for the 3.8 mm and

1.9 mm thick impactors, respectively. Velocities of .10 mm/μsec and .12 mm/μsec were required to create complete separation or spallation in the thick and thin CVD felt targets. The spall data are plotted in Figure 19, with impact velocity plotted as a function of impactor thickness.

The impact stress amplitudes generated in the spall experiments were calculated using the Hugoniot data. For the incipient spallation condition, impact stresses of approximately 0.8 and 1.0 kbar were generated in the 7.6 mm and 3.8 mm thick targets, respectively. It should be emphasized, however, that these values are not necessarily the amplitudes of the tensile pulses that were present in the targets, because of pulse dispersion and attenuation in the very low stress region. Further discussion of these points will be covered in the discussion section, where a comparison is made with these data and earlier results on porous carbons.

IV. Discussion

A general comparison was made of the current results on the flight quality CVD felt with similar data on other carbon-carbon materials of engineering interest. This comparison made a more comprehensive evaluation of the distended carbon felt's shock behavior possible. The stress wave attenuation and spallation characteristics were two important areas of material response that were considered.

Stress wave attenuation in the CVD carbon felt was considerably more pronounced than that observed in previously studied porous carbon-carbon materials of approximately the same density.[21] The two main factors that produced the enhanced attenuation in the flight quality felt were: (1) the high compressibility, which resulted in slow compaction wave velocities and; (2) the steep initial unloading paths, which produced very fast relief waves. The

compressibility of the CVD felt in the partially compacted region was a factor of 5 to 10 larger than similar porous carbons that have been studied. The measured release wave speeds in the current felt were also faster than those previously observed. Consequently, rarefaction wave catch up and attenuation for a given shock pulse occurred much quicker in the CVD felt than in the other distended carbons.

The CVD carbon felt spallation data are directly compared in Figure 20 with the previous spall results on other distended carbons. The earlier spall data used in the comparison are summarized in Table VI. As shown by Figure 20, the impact velocity necessary to create spall damage in the flight quality CVD felt was substantially higher than that required for most of the other porous carbon-carbon materials. One must remember, however, that the parameter of interest for comparison purposes is the dynamic tensile strength of the various materials. Unfortunately this cannot be measured directly, but must be inferred from wave propagation calculations which are based on a constitutive model. The calculated spall strengths for all the carbons in Figure 20 except the flight quality CVD felt and the ST-17300 material were in the 0.3 to 1.0 kbar range, based on the assumption of linear elastic response. It was clear from the shock compaction data that this type of analysis does not apply to the CVD felt and its applicability to some of the other materials was questionable. If one ignores the complex response illustrated by this investigation and assumes an elastic response, the calculated CVD felt incipient spall strengths would be 1.8 and 2.5 kbars for the 3.8 and 1.9 mm thick impactors, respectively. These values of spall strength for the CVD felt were approximately the same as those reported for the ST-17300 porous carbon.[26] Based on the present comparison of spall data, the spall resistance of the flight quality carbon felt appeared to be equal to or better than the other porous carbon materials investigated.

The spall data plotted in Figure 20 also indicate that for spallation to occur, the impact velocity must increase as the impactor and pulse width become thinner. Time dependent spallation behavior has been observed in other materials, principally metals. The effect of rate dependent spall behavior would be an increase in spall strength for shorter applied stress pulses. Thus, for pulses of shorter duration than those used in this investigation (about 2.0 μsec), a higher impact velocity would be expected.

V. CONCLUSIONS

The shock response of flight quality CVD carbon felt has been experimentally characterized from the shock compaction, release, and spallation data. The equation-of-state parameters for modeling the shock response of the CVD felt were derived from the experimental results. These material parameters, when applied to the P-α model, were found to adequately predict attenuation response. It has been shown that the computational assumption of linear release paths used in the model was not physically realistic for the felt in the low stress region (below 1.0 kbar) because it did not allow for the significant void recovery observed in the material. However, the effect of this discrepancy was minimal for the calculations made in this investigation and is only expected to be important for stress wave calculations below 1.0 kbar.

The static one-dimensional strain results agreed in general with the shock data, indicating the applicability of the static technique to estimate the shock compaction and release response of rate-insensitive porous carbon materials. This technique made possible the measurement of portions of unloading paths that could not be determined in the shock experiments.

The qualitative material damage results from the ultrasonics and SEM work showed some internal material damage due to static compaction to 5.1 kbar.

However, the damage was on a localized scale adjacent to the pores and was not spread throughout the bulk solid material. The internal material damage resulting from effectively total void closure in the CVD felt was minimal and probably contributed to the observed high spall resistance.

A comparison of the experimental results with data for similar materials showed that the flight quality felt was a better shock mitigator and had higher spall resistance than the previously studied carbon-carbon materials. The enhanced attenuation resulted from the unique shock compaction and release behavior of the carbon felt, which was similar to that observed for pressed graphites (ATJ and LASL).[23,24]

REFERENCES

1. Irwin, J. L., "An Evaluation of Felt Substrate and Processing Parameters for a Chemical Vapor Deposited (CVD) Carbon Composite Material," Sixteenth National SAMPE Symposium, Vol. 16, Materials '71, April 1971, pp. 190-204.
2. Memo from B. Granoff, 5315, to J. L. Irwin, 1225, Subject: Microstructural Analysis of SAMAST Heat Shields, Sept. 8, 1970.
3. Mantell, C. L., Carbon and Graphite Handbook, Interscience, New York, 1968.
4. Johnston, J. K., Sandia Laboratories, Private Communication.
5. Rice, M. H., McQueen, R. G., and Walsh, J. M., in Solid State Physics, "Compression of Solids by Strong Shock Waves," F. Seitz and D. Turnbull, Eds., Academic Press, Inc., New York, 1958, Vol. 6, pp. 1-63.
6. Barker, L. M., and Hollenbach, R. E., "System for Measuring the Dynamic Properties of Materials," Review of Scientific Instruments, Vol. 35, No. 6, 1964, pp. 742-746.
7. Graham, R. A., Neilson, F. W., and Benedick, W. B., "Piezoelectric Current From Shock-Loaded Quartz - A Submicrosecond Stress Gauge," Journal of Applied Physics, Vol. 36, No. 4, 1965, pp. 1775-1783.
8. Barker, L. M., and Hollenbach, R. E., "Shock-Wave Studies of PMMA, Fused Silica, and Sapphire," Journal of Applied Physics, Vol. 41, No. 10, Sept. 1970, pp. 4208-4226.
9. Butcher, B. M., and Cannon, J. R., "Influence of Work-Hardening on the Dynamic Stress-Strain Curves of 4340 Steel," AIAA Journal, Vol. 2, No. 12, Dec. 1964, pp. 2174-2179.
10. Karnes, C. H., Sandia Laboratories, Private Communication.

11. Lysne, P. C., Boade, R. R., Percival, C. M., and Jones, O. E., "Determination of Release Adiabats and Recentered Hugoniot Curves by Shock Reverberation Techniques," Journal of Applied Physics, Vol. 40, No. 9, August 1969, pp. 3786-3795.

12. Barker, L. M., and Hollenbach, R. E., "Interferometer Technique for Measuring the Dynamic Mechanical Properties of Materials," Rev. Sci. Inst. 36, p. 1617, 1965.

13. Halpin, W. J., Jones, O. E., and Graham, R. A., in ASTM Spc. Publ. No. 336, p. 208.

14. Prepared by Group GMX-6, Selected Hugoniots, LASL Report No. LA-4167-MS, May 1, 1969.

15. The rigid carbon foam backing was a .26 gm/cm^3 material on which low stress Hugoniot and release wave data have been generated. The entire results of this study will be documented in a future report. The σ_x, u_p relation used to describe the foam in this work was $\sigma_x = 1.03\ u_p + 2.46\ u^2_p$ (units are kbar and mm/μsec).

16. Keough, D. D., "Procedure for Fabrication and Operation of Manganin Shock Pressure Gages," AFWL-TR-68-57, August 1968.

17. Keough, D. D., and Wong, J. Y., "Variation of the Shock Piezoresistance Coefficient of Manganin as a Function of Deformation," Journal of Applied Physics, Vol. 41, No. 8, July 1970, pp. 3508-3515.

18. Pulsar Instruments, Redwood City, California.

19. Burchett, O. L., "An Evaluation of a Laterally Confined Isothermal Test Technique to Estimate the Shock Behavior of Low-Strength Materials," Dissertation to University of Oklahoma, 1969, Doctor of Engineering.

20. Mattaboni, P., and Schreiber, E., "Method of Pulse Transmission Measurements for Determining Sound Velocities," Journal of Geophysical Research, Vol. 72, No. 7, 1969, p. 2967.

21. Lee, L. M., May, R. P., Guess, T. R., "Some Dynamic Mechanical Properties of Distended Carbons," AIAA Journal, Vol. 8, No. 8, August 1970, pp. 1421-1428.

22. Herrmann, W., "Equation of State of Crushable Distended Materials," SC-RR-66-2678, Sandia Laboratories, March 1968.

23. Linde, R. K., and Schmidt, D. N., "Shock Propagation in Nonreactive Porous Solids," Journal of Applied Physics, Vol. 37, No. 8, July 1966, pp. 3259-71.

24. Charest, J. A., "Measurements of Spall Thresholds and Stress Wave Characteristics in 1.76 g/cc Graphite," EG&G, Inc. Technical Report S-549-R, August 1971.

25. Lawrence, R. J., and Mason, D. S., "WONDY IV - A Computer Program for One-Dimensional Wave Propagation With Rezoning," SC-RR-710284, August 1971.

26. Horne, D. E., Charest, J. A., and Jenrette, B. D., "Spall Thresholds of Selected Carbon Materials," EG&G, Inc., Technical Report S-460-R, June 1969.

27. Gauster, W. B., "Elastic Constants and Grüneisen Parameters of Pyrolytic Graphite," Phil. Mag., Vol. 25, p. 687, 1972.

28. Warnica, R. L., "Spallation Thresholds of S-200 Beryllium, ATJ-S Graphite and Isotropic Boron Nitride at 75°F, 500°F and 1000°F," MSL, Manufacturing Development, GM Corp., MSL-68-18, July 1968.

29. Guess, T. R., and Lee, L. M., "Spall Strengths of Five Carbon Materials," SC-DR-68-604, Sandia Laboratories, October 1968.

Table I. Summary of Hugoniot and Release Adiabat Data for Flight Quality CVD Carbon Felt

Initial Conditions				Hugoniot States				Release Adiabat States		
ρ_o (g/cm^3)	V_L* (mm/μsec)	Type of ** Experiment	Imp. Vel. (mm/μsec)	σ_x (kbar)	u_p (mm/μsec)	U (mm/μsec)	v (cm^3/g)	σ (kbar)	u (mm/μsec)	$\overline{U}_R^+$ (mm/μsec)
1.73++	2.67	1	----	.3	.010	1.73	.575	----	----	----
1.76	----	2(a)	.078	1.2	.070	.85	.525	.88 .77	.060 .056	1.54
1.75	----	2(a)	.154	2.2	.139	.84	.480	1.52 1.34	.123 .119	2.20
1.71	----	2(b)	.150	2.4	.145	.90	.495	1.82	.130	1.82
1.72	2.64	1	.154	2.6	.149	.96	.494	----	----	----
1.72	2.68	1	.215	3.5	.208	.93 1.00†	.456	----	----	----
1.72	----	2(a)	.310	5.6	.273	1.16	.448	3.27	.237	2.88
1.72	2.76	1	.274	6.0	.260	1.32 1.31†	.468	----	----	----
1.80	----	2(b)	.276	6.7	.261	1.41	.454	4.50 3.50	.234 .220	3.60
1.76	2.79	3(b)	.344	9.4	.323	1.64	.457	----	----	----
1.74	2.80	3(b)	.390	10.4	.367	1.62	.445	----	----	----
1.70	2.64	1	.372	10.5	.350	1.75 1.65†	.471	----	----	----
1.71	2.64	1	.428	12.1	.401	1.75 1.79†	.452	----	----	----
1.72	2.70	3(a)	.580	14.3	.465	1.78	.430	----	----	----

TABLE I

(continued)

Initial Conditions				Hugoniot States				Release Adiabat States		
ρ_o (g/cm^3)	V_L* (mm/μsec)	Type of ** Experiment	Imp. Vel. (mm/μsec)	σ_x (kbar)	u_p (mm/μsec)	U (mm/μsec)	v (cm^3/g)	σ (kbar)	u (mm/μsec)	$\bar{U}_R^+$ (mm/μsec)
1.69	2.53	3(a)	.588	15.0	.468	1.88	.446	----	----	----
1.79	2.67	3(a)	.587	16.0	.458	1.95	.427	----	----	----
1.76	2.70	3(c)	.646	29.5	.618	2.71	.438	----	----	----
1.70	2.46	4(a)	----	51.4	1.013	2.98	.388	----	----	----
1.74	2.66	4(b)	----	81.5	1.227	3.81	.389	----	----	----
1.79	2.59	4(c)	----	145.	1.735	4.66	.350	----	----	----
1.74	2.74	4(d)	----	162.	1.856	5.00	.361	----	----	----

*Ultrasonically measured longitudinal velocity.

**Type of experiment:

1. transmitted wave profile using a double-quartz gauge technique.
2. shock reverberation technique using (a) thin quartz crystal reverberation plate; (b) thin $4340R_c54$ steel reverberation plate with a displacement interferometer.
3. sample impacting a buffer plate of (a) fused silica; (b) $4340R_c54$ steel; (c) tungsten carbide.
4. explosive loading using a copper driver plate and (a) Barstol; (b) TNT; (c) Comp. B, and (d) PBX 9404.

+Average release wave speed calculated from the linear release adiabat slope.

++Average precursor data from all the transmitted wave experiments; average σ_x, ρ_o and U (U at half amplitude of precursor ramp).

†Measured compaction wave velocity at half amplitude.

Table II. Parameters Used to Model the Flight Quality CVD Carbon Felt in WONDY IV Calculations

Parameter	Solid Material	Distended CVD Felt
ρ_o (g/cm^3)	2.17	1.73
C_o (mm/μsec)[21]	3.90	-
S	2.20	-
Γ_o[27]	.25	-
P_s (kbar)	-	5.0*
P_e (kbar)	-	.3
C_e (mm/μsec)	-	1.73

* A quadratic P-α relations was used.

Table III. Summary of Experimental Parameters from Attenuation Experiments on Flight Quality CVD Carbon Felt

Specimen Description				Impactor Description				
Target Thickness (mm)	Initial Density (g/cm^3)	V_L* (mm/μsec)	Type of Transducer	Impactor Material	Impactor Thickness** (mm)	Impact Velocity (mm/μsec)	Tilt (Rad. x 10^3)	Impact Stress† (kbar)
2.05	1.80	-	Manganin	Fused Silica	1.68	.5847	1.0	16.
2.10	1.66	-	Manganin	Fused Silica	1.68	.5854	1.1	15.
4.09	1.79	2.56	Manganin	Fused Silica	1.70	.5860	.8	16.
6.41	1.66	2.54	Manganin	Fused Silica	1.69	.5842	.9	15.0

* Ultrasonically measured longitudinal velocity

** Each impactor plate was backed with a 5.0 mm thick disk of carbon foam.[15]

† Measured impact stress from separate experiments where a CVD felt sample impacted a fused silica buffer plate at .580 to .588 mm/μsec.

Table IV. Summary of Static Compression Test Results on Flight Quality CVD Carbon Felt

Sample Number	Density (g/cm^3)	Number of Load Cycles[+]	Pre-Comp. Test V_L[*] (mm/μsec)	Post-Comp. Test V_L (mm/μsec)	Max. Strain (%)	Permanent Strain (%)
7	1.71	1	2.53	1.79	18.8	4.3
8	1.73	3	2.52	1.60	17.7	5.5
9	1.72	3	2.66	1.71	18.6	4.4
10	1.71	3	2.61	1.74	17.2	5.0

[+]Load released at intermediate points and then reloaded. Maximum load was 5.1 kbars obtained on last cycle.

[*]Ultrasonically determined longitudinal wave speed before static test.

Table V. Spallation Data for Flight Quality CVD Carbon Felt

Impactor*			Target		
Imp. Vel (mm/μsec)	Thickness (mm)	Density (g/cm^3)	Thickness (mm)	Density (g/cm^3)	Fracture Level
.050	3.86	1.72	7.68	1.63	No Damage
.063	3.89	1.72	7.70	1.71	No Damage
.072	3.86	1.80	7.67	1.80	No Damage
.076	3.86	1.78	7.71	1.78	No Damage
.086	3.89	1.76	7.70	1.77	Micro-cracks linked up (10 to 20X)
.093	3.86	1.70	7.70	1.72	Micro-cracks linked up (1 to 10X)
.103	3.86	1.76	7.70	1.72	Complete Spall
.087	1.98	1.72	3.86	1.75	No Damage
.095	1.98	1.77	3.89	1.77	No Damage
.103	1.98	1.82	3.87	1.83	No Damage
.114	1.91	1.69	3.86	1.68	Micro-cracks, not linked up (1-10X)
.117	1.98	1.65	3.87	1.66	Micro-cracks, not linked up (10-20X)
.121	1.98	1.67	3.89	1.67	Complete Spall

* All the data were generated using symmetric impacts, with free rear surfaces on the impactor and target.

Table VI. Spallation Data for Porous Carbons and Graphites

Material	Density (g/cm^3)	Longitudinal Velocity (mm/μsec)	Impactor Thickness[1] (mm)	Impact Velocity[2] (mm/μsec)	Fracture Level	Source
ATJ-S	1.80	2.60	.81 1.60 3.18	.055- .044- .035-.041	Microcracks at 100X Microcracks at 100X to macrocracks at 1X	Ref. 28
LASL	1.76	2.20	1.27 2.03	.040-.050 .026-.040	Microcracks at 50-200X Microcrack at 0-200X to microcracks at 1-10X	Ref. 24
ST-17100[3]	1.76	3.66	1.27 2.54	.041-.053 .023-.030	Microcracks at 50-200X to macrocrack at 1-10X	Ref. 26
ST-17300[3]	1.84	2.26	1.27 2.54	.155-.195 .085-.114	Microcracks at 50-200X to macrocracks at 1-10X	Ref. 26
ST-WOOL[3]	1.5	1.47	2.54	.052-.062	Microcracks at 50-200X to macrocracks at 1-10X	Ref. 26
CF-CVD-U CF-CVD-G BKC-1 BKC-3 BKC-4	1.76 1.71 1.40 1.34 1.40	2.70 2.10 3.34 3.58 3.40	4.70 4.78 4.57 4.57 4.70	.040-.046 .055-.061 .020-.030 .015-.027 .035-.038	No visible cracks on the sample circumference to partial separation (macrocracks)	Ref. 21
C/S-0	1.65	3.50	2.54	.021-.027	No visible cracks on the sample circumference to complete separation	Ref. 29

[1] Target to thickness ratio was 2:1.

[2] All the data were generated using symmetric impacts.

[3] Impactors were backed by .064 g/cm^3 rigid polyurethane foam.

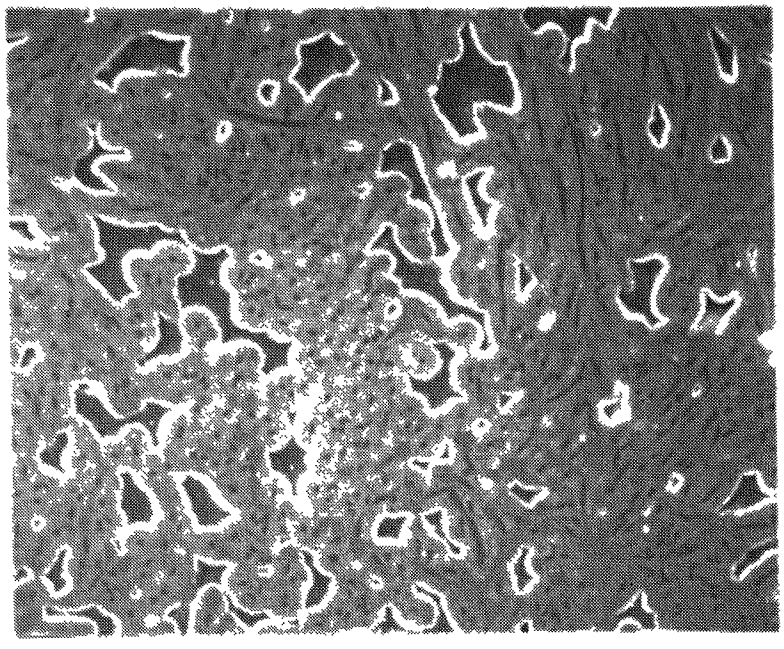

1 (a)
100x

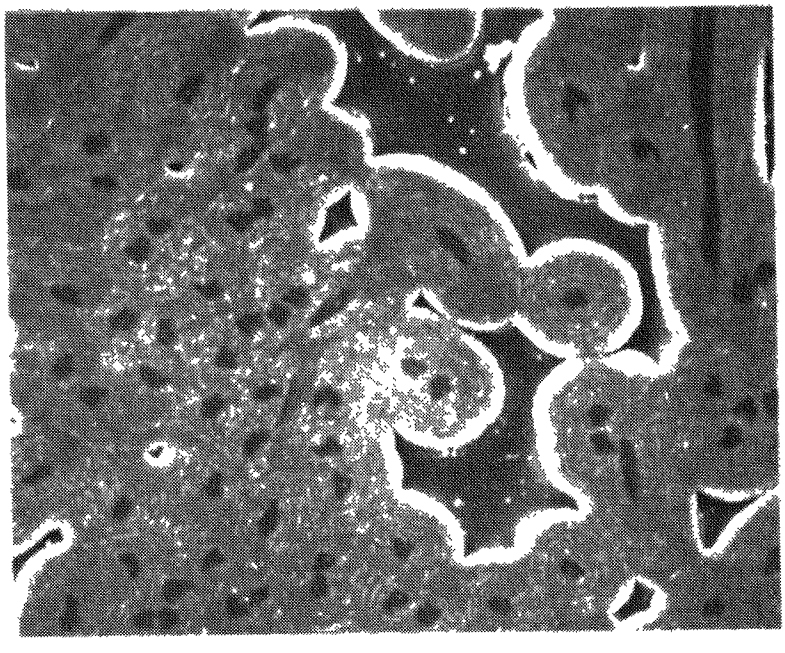

1 (b)
300x

FIGURE 1. SEM RECORDS SHOWING THE TYPE OF PORE STRUCTURE PRESENT IN THE CVD CARBON FELT

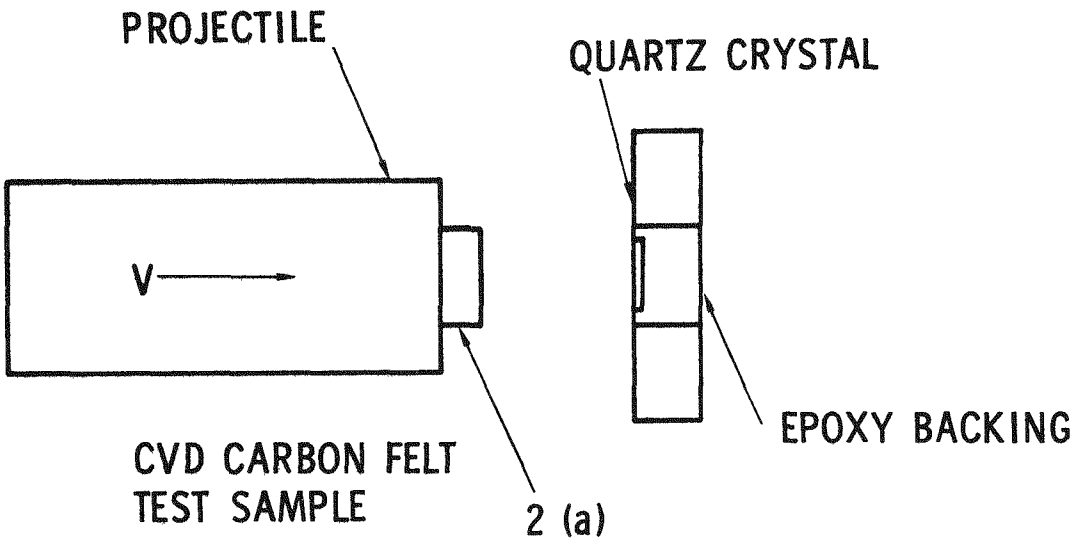

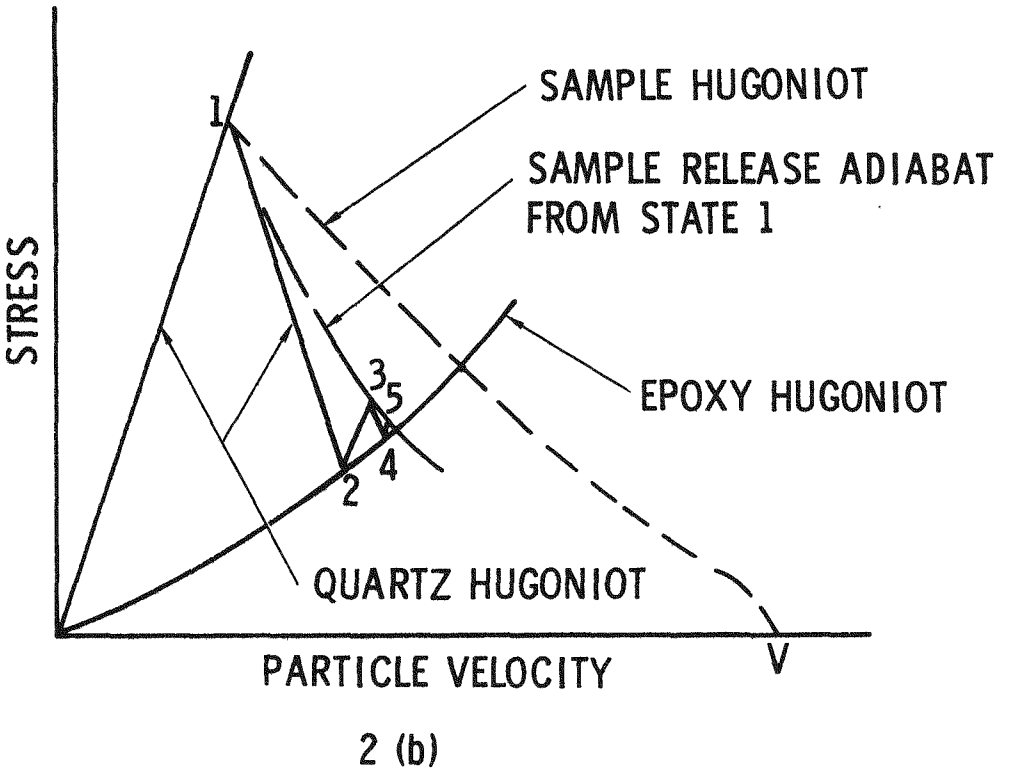

FIGURE 2. SCHEMATIC DIAGRAM OF A RELEASE EXPERIMENT USING A QUARTZ SHOCK REVERBERATION TECHNIQUE

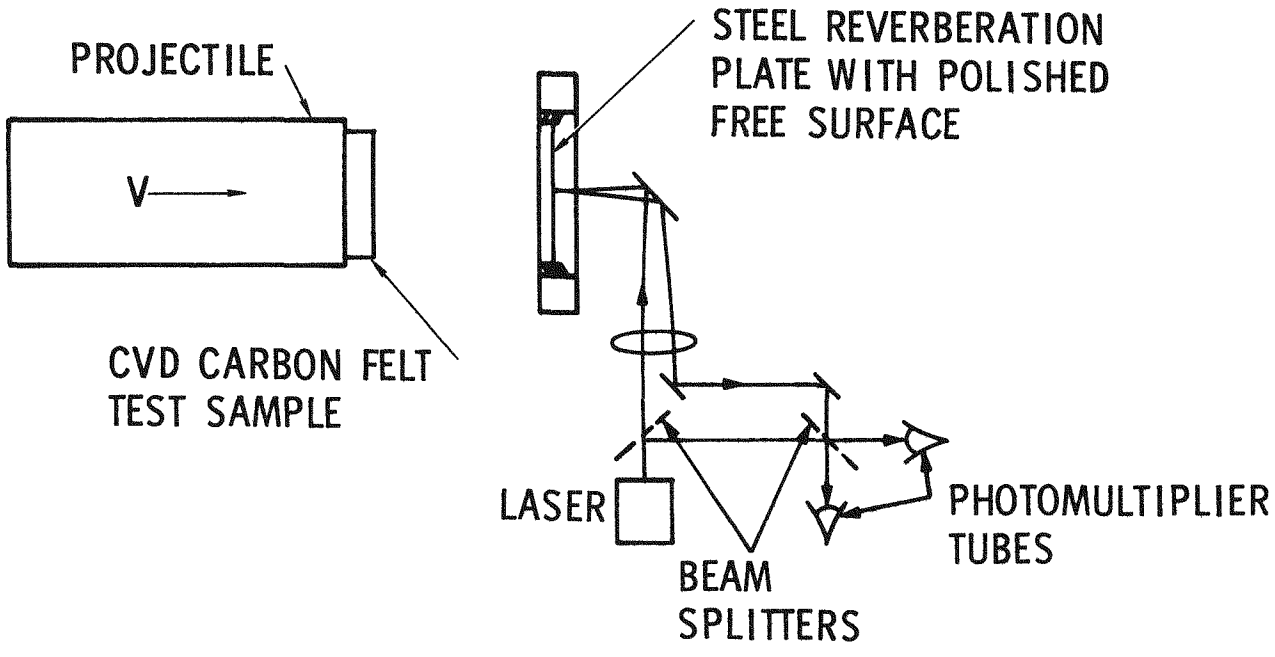

3 (a)

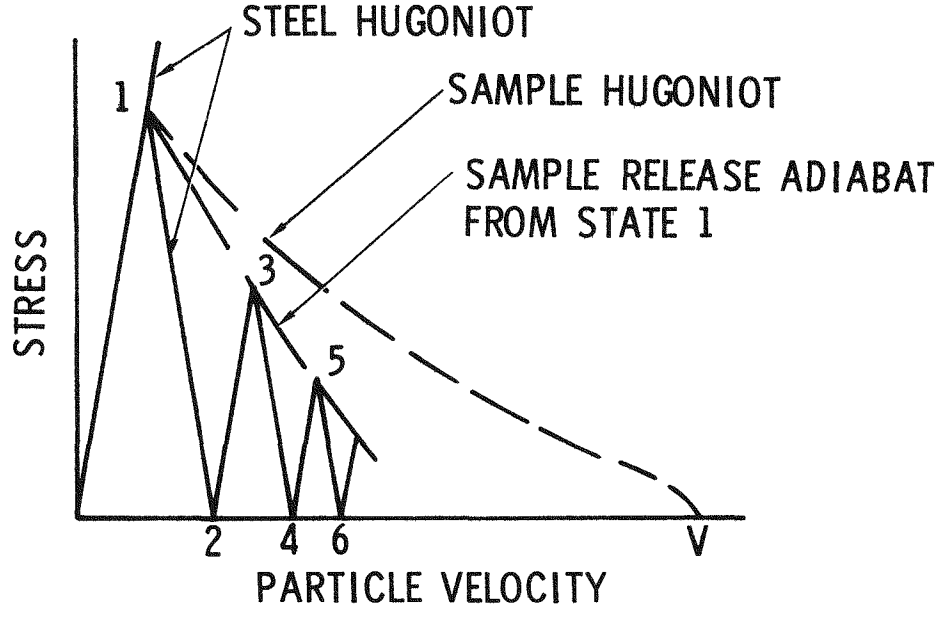

3 (b)

FIGURE 3. SCHEMATIC DIAGRAM OF A RELEASE EXPERIMENT USING A STEEL REVERBERATION PLATE AND DISPLACEMENT INTERFEROMETER

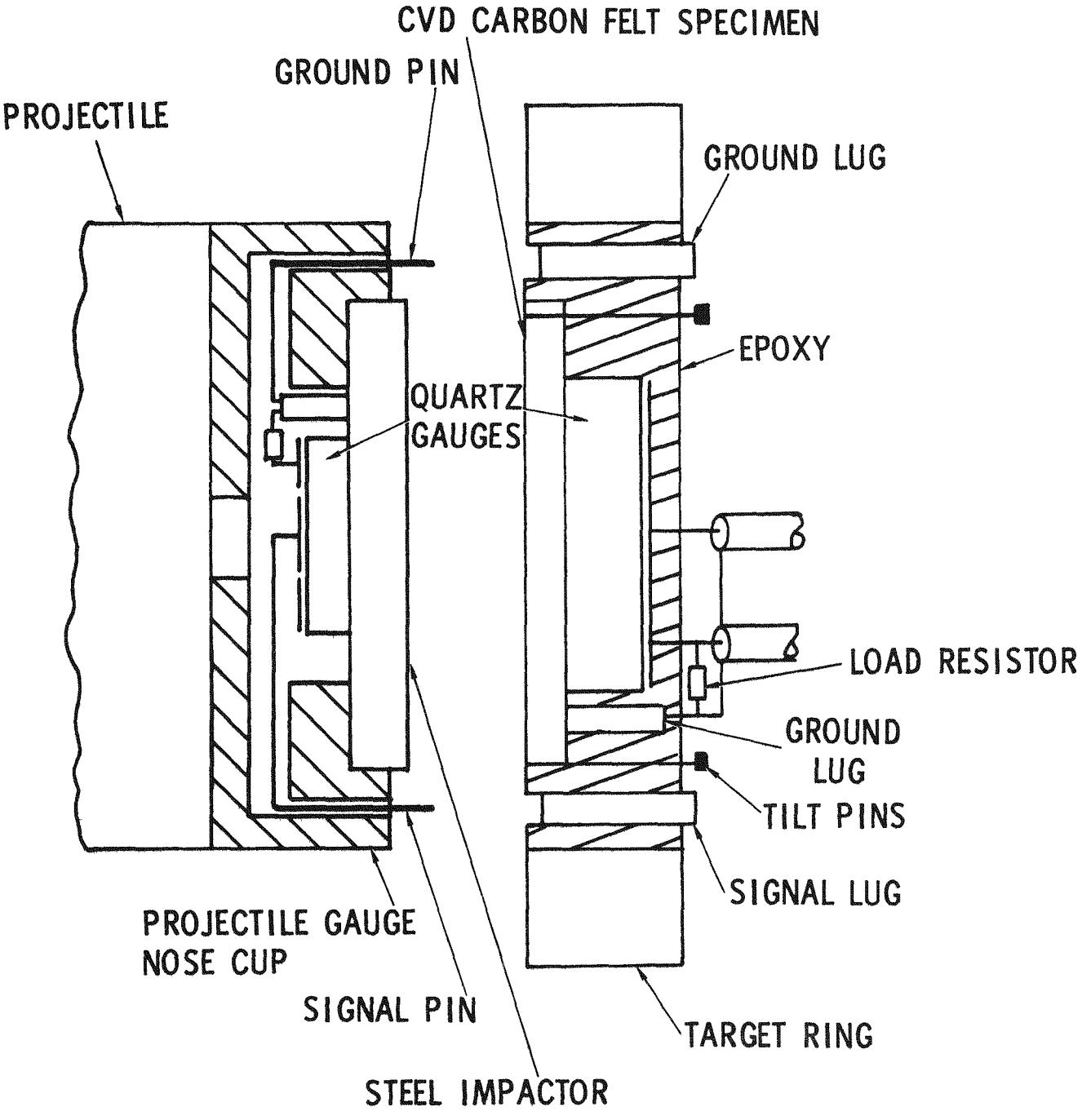

FIGURE 4. SCHEMATIC DIAGRAM OF A TRANSMITTED WAVE EXPERIMENT

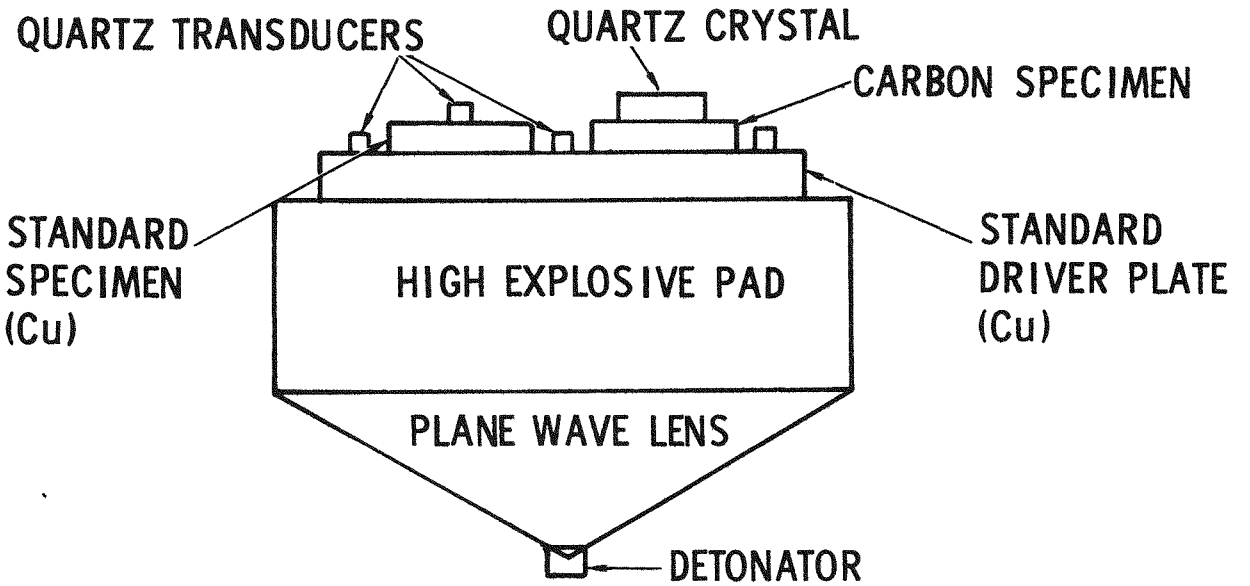

FIGURE 5. SCHEMATIC OF AN EXPLOSIVE EXPERIMENT USED TO GENERATE HIGH STRESS HUGONIOT DATA

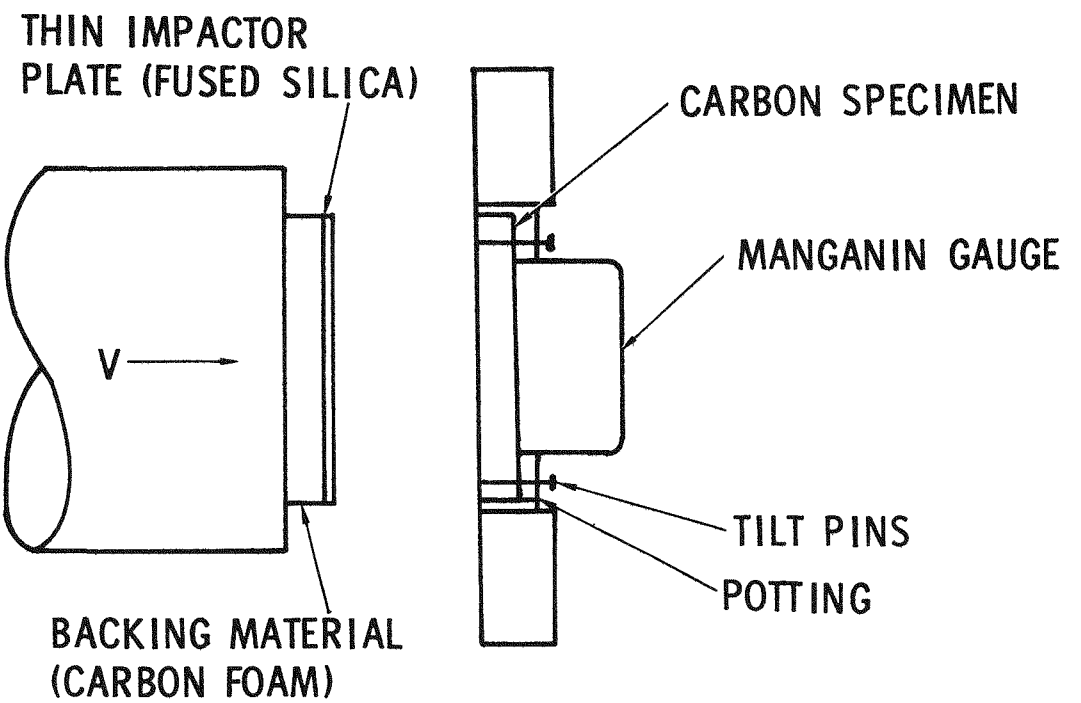

FIGURE 6. CONFIGURATION USED FOR THE ATTENUATION EXPERIMENTS

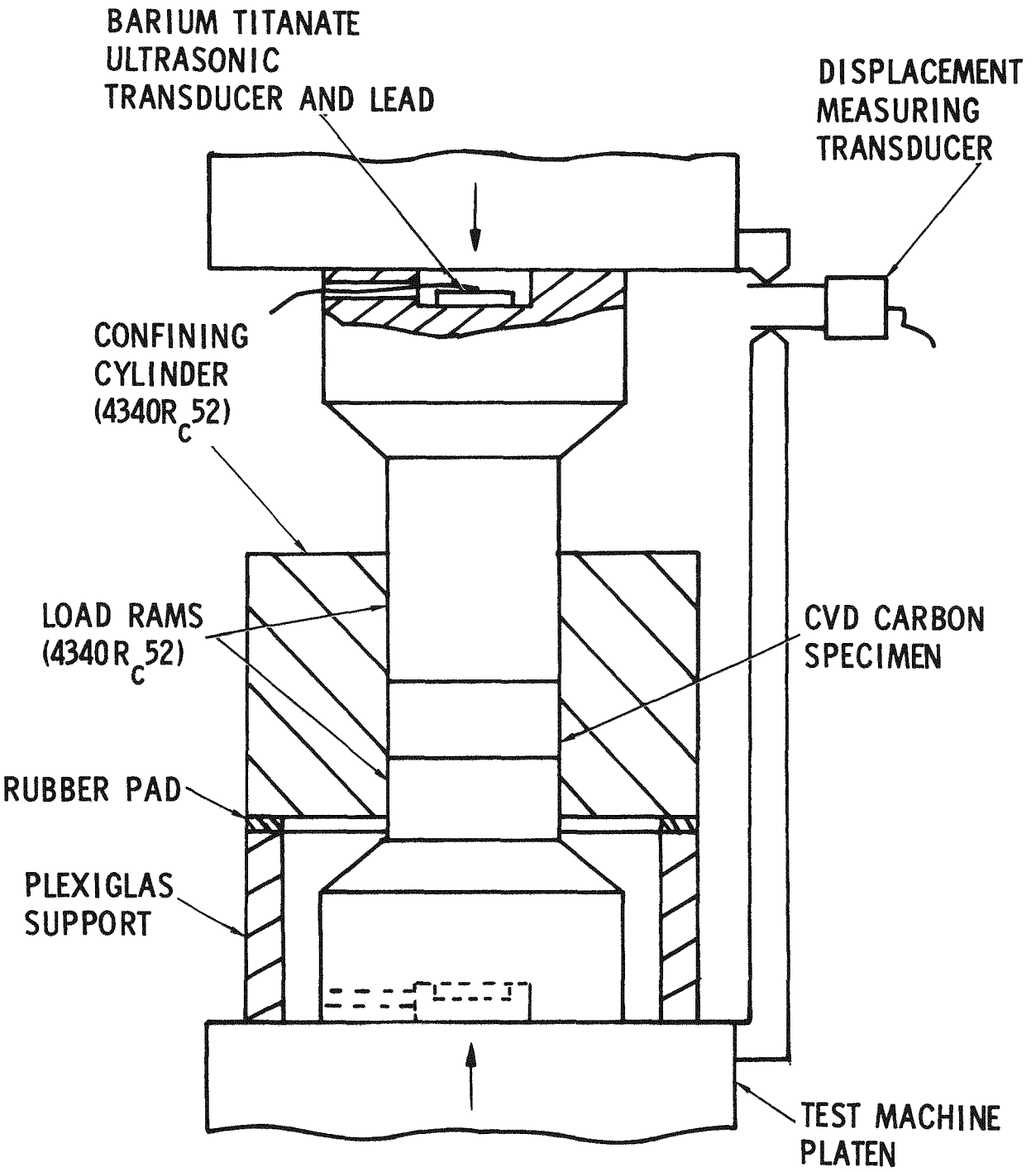

FIGURE 7. TEST CONFIGURATION FOR STATIC LATERALLY CONSTRAINED COMPRESSION EXPERIMENTS WITH ULTRASONIC VELOCITY MEASUREMENTS

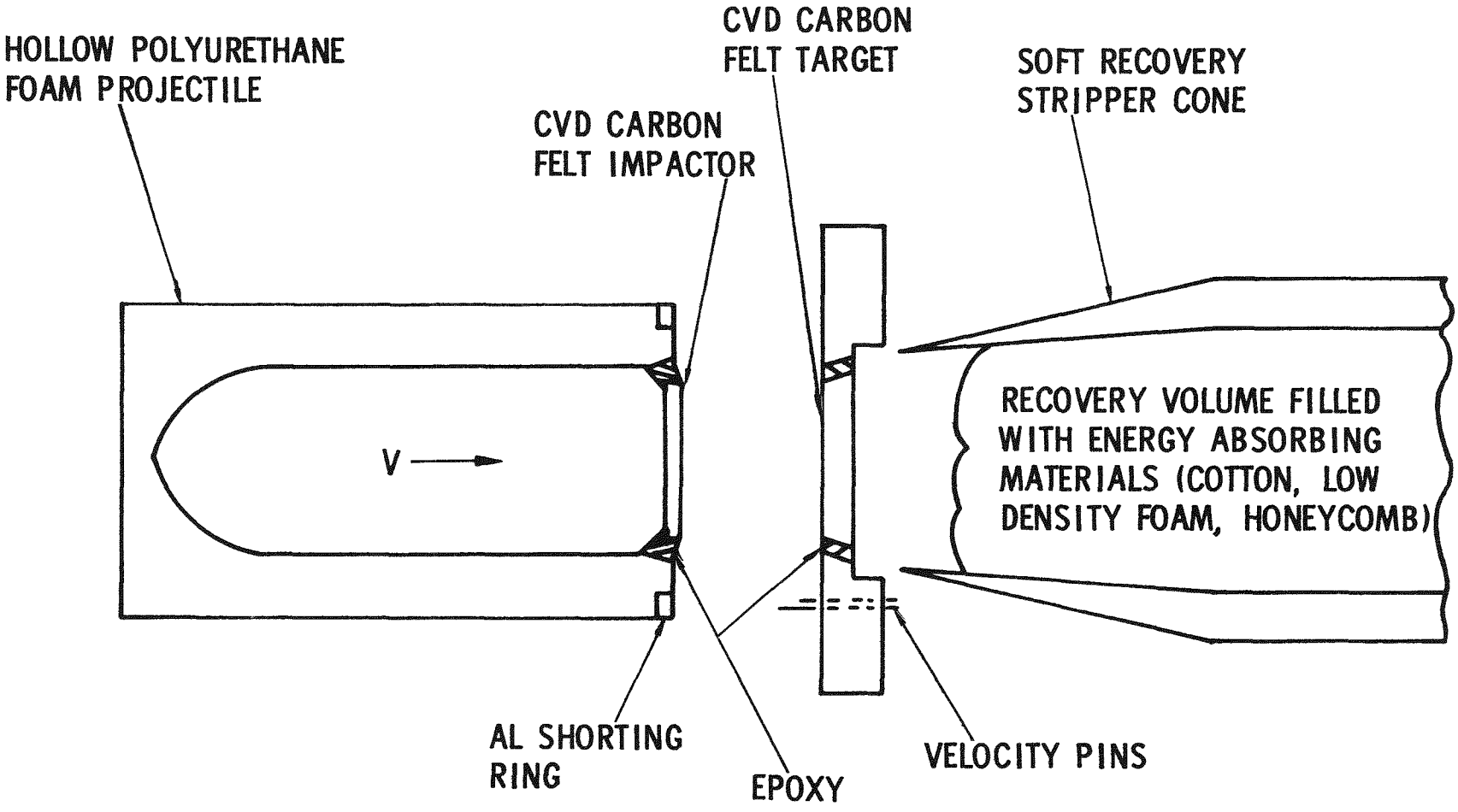

FIGURE 8. CONFIGURATION USED FOR THE SPALLATION EXPERIMENTS

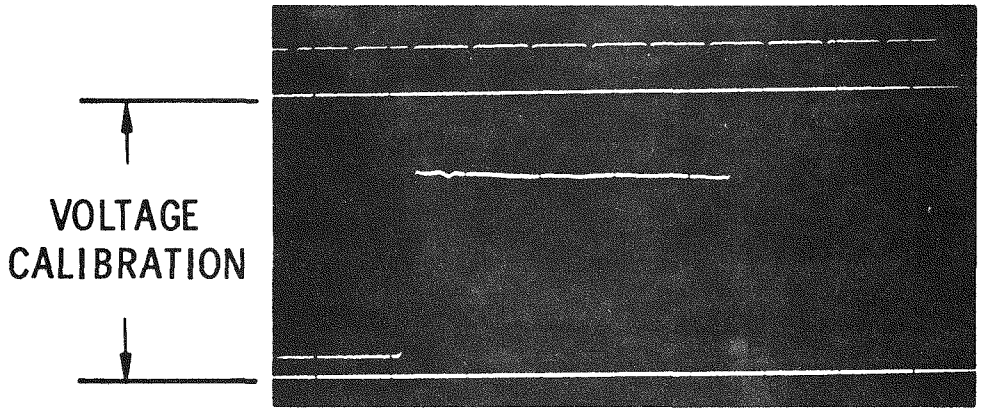

9 (a)

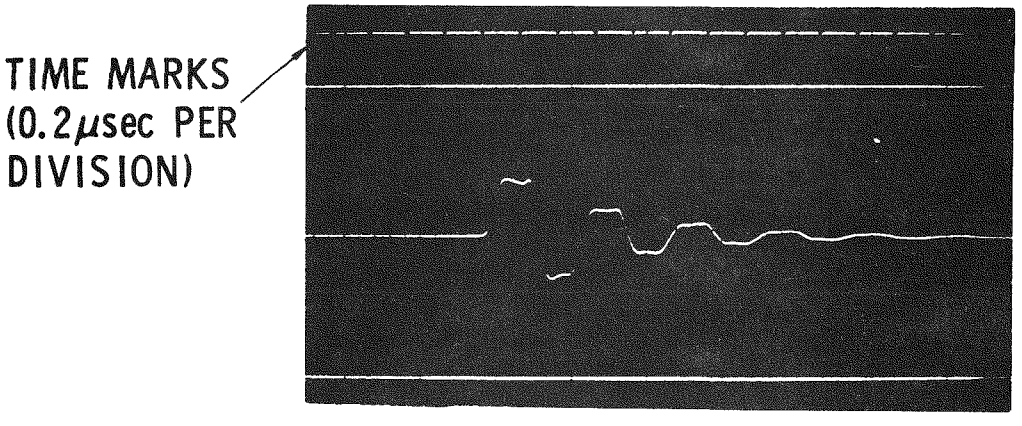

9 (b)

FIGURE 9. QUARTZ GAUGE RECORDS FROM
(a) 4340 STEEL BUFFER PLATE, AND
(b) REVERBERATING WAVE EXPERIMENTS

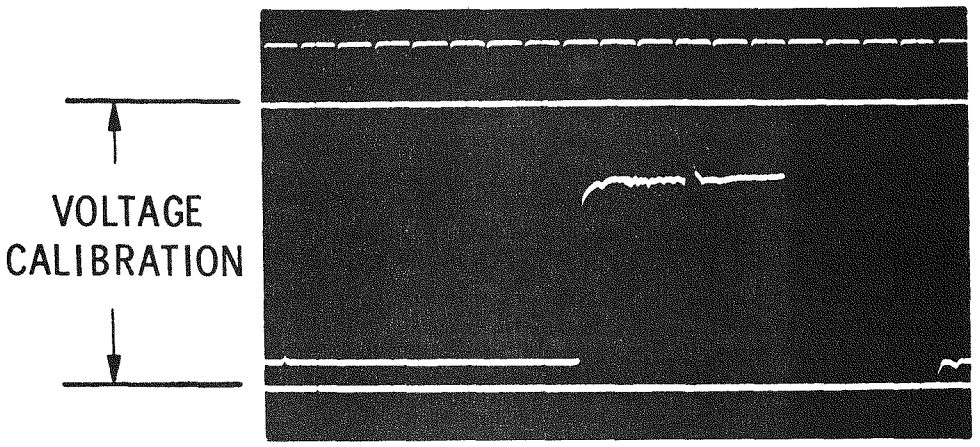

10(a)

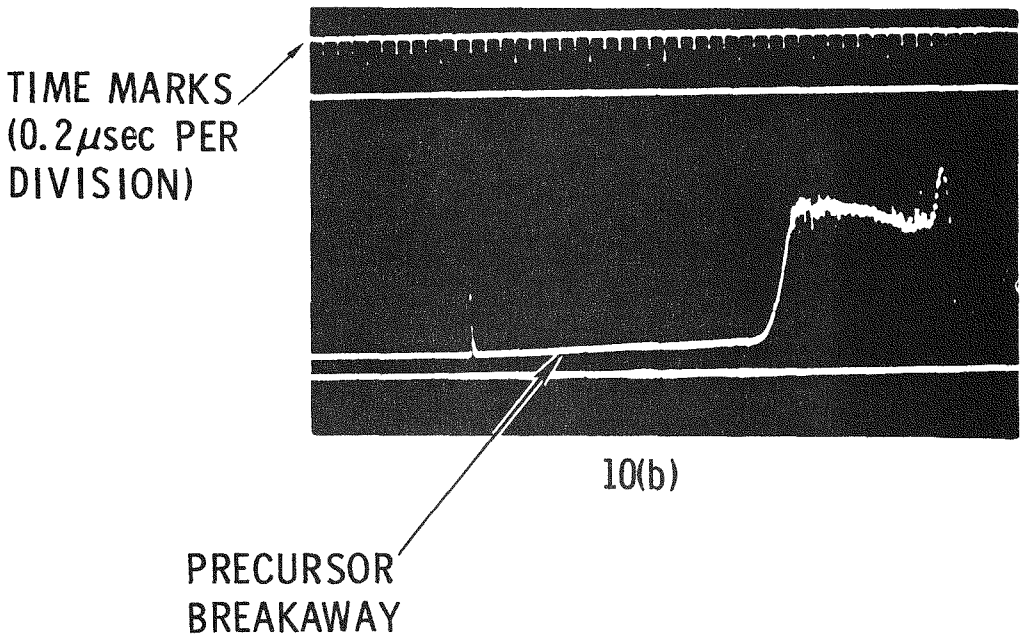

10(b)

FIGURE 10. QUARTZ RECORDS FROM A DOUBLE GAUGE TRANSMITTED WAVE EXPERIMENT. PROJECTILE GAUGE IS 10(a) AND THE TARGET GAUGE IS 10(b). NOTE THE SLIGHT RAMP PRIOR TO THE COMPACTION WAVE IN 10(b). THE SPIKE IN 10(a) AND 10(b) IS A FIDUCIAL MARKER.

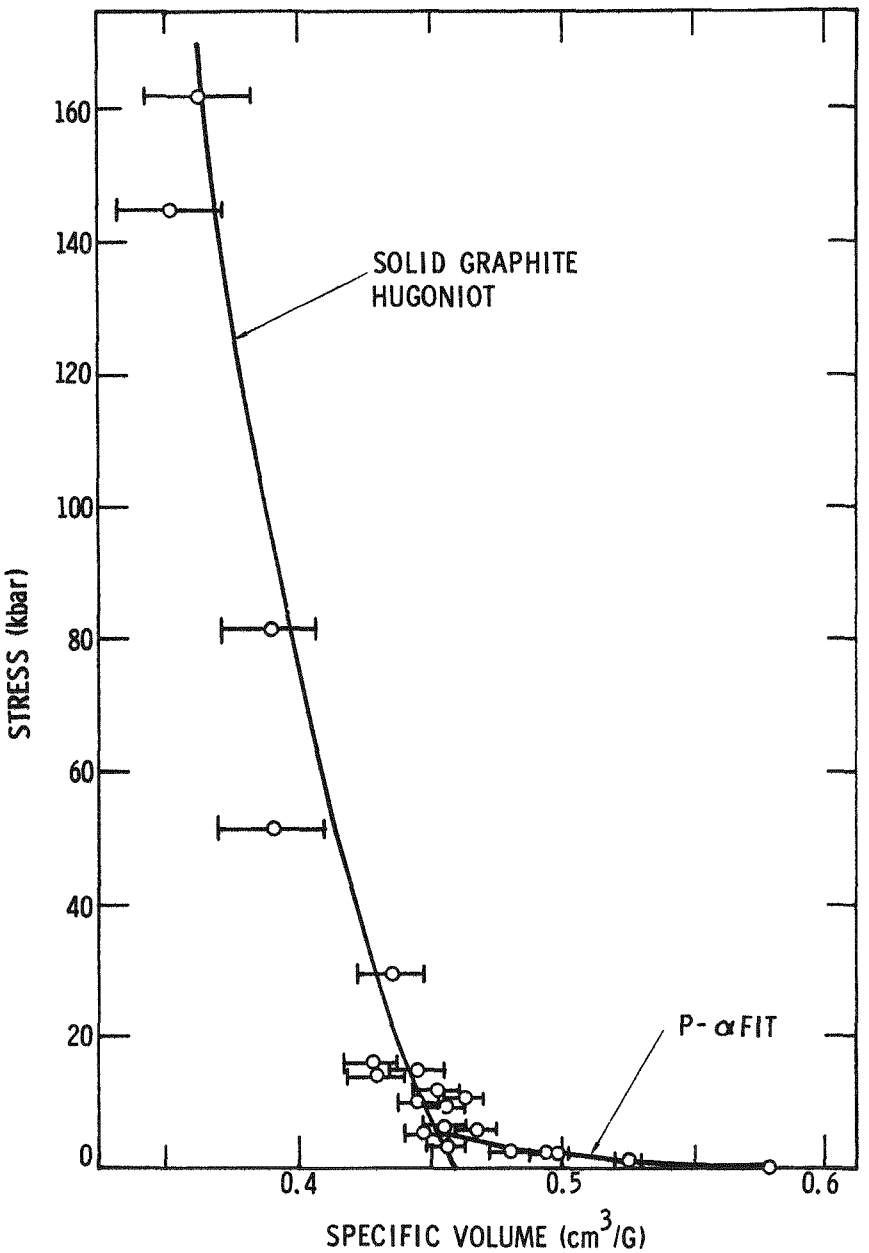

FIGURE 11. CVD CARBON FELT HUGONIOT DATA

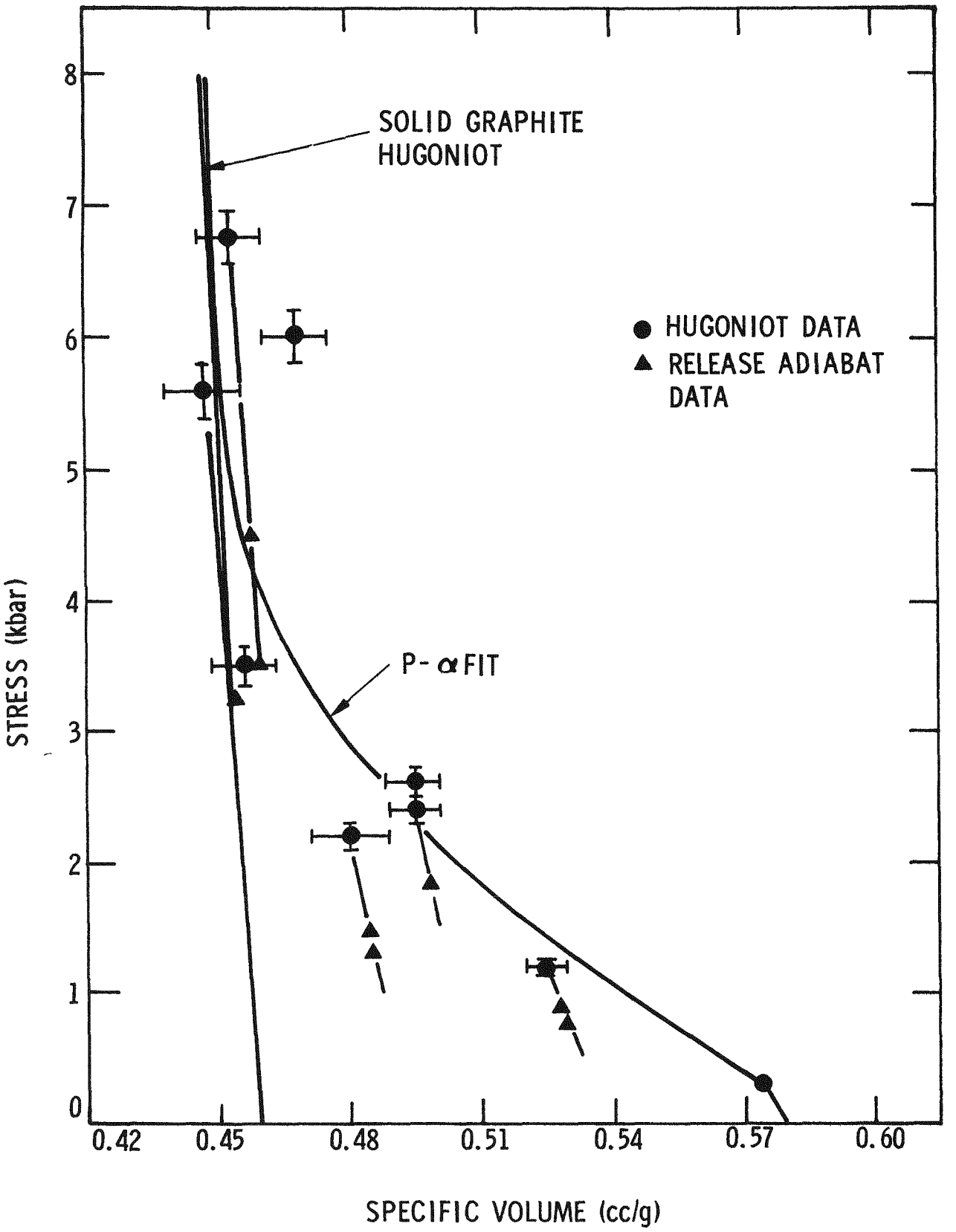

FIGURE 12. CVD CARBON FELT HUGONIOT AND RELEASE ADIABAT DATA

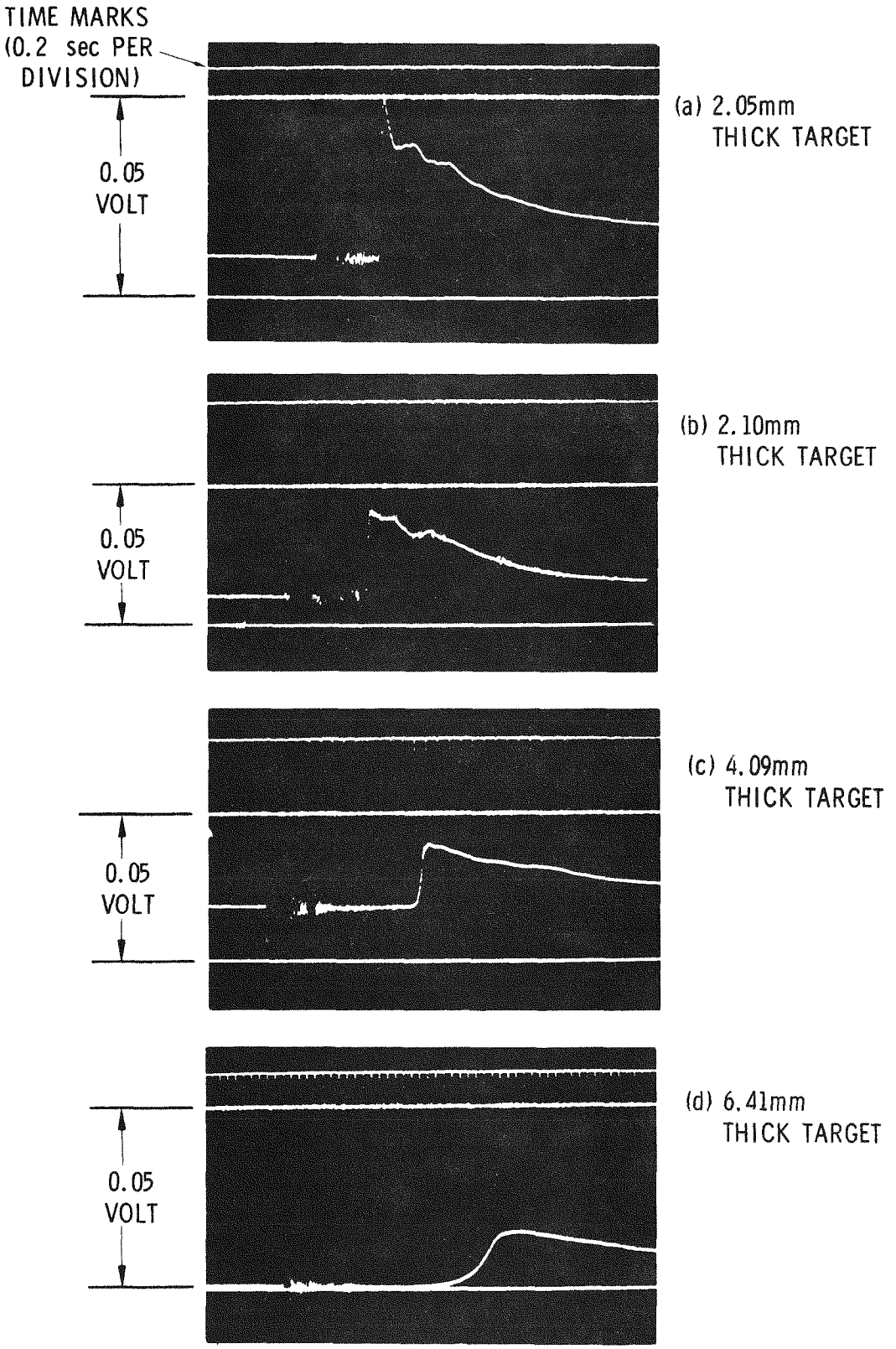

FIGURE 13. ATTENUATED WAVE PROFILE MEASUREMENTS FOR CVD CARBON FELT USING MANGANIN TRANSDUCERS

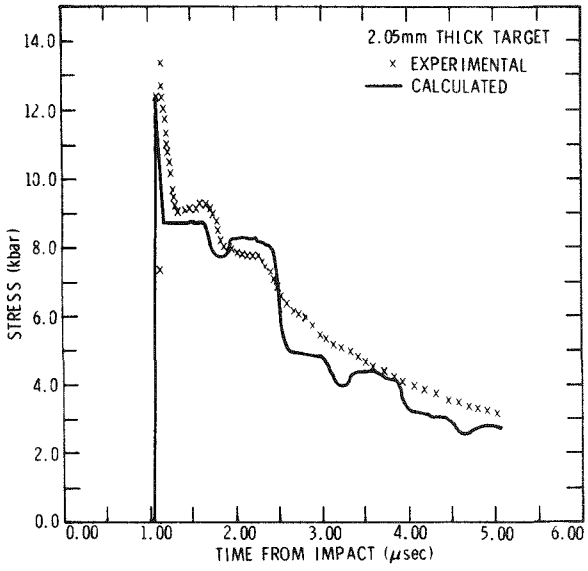

14(a)

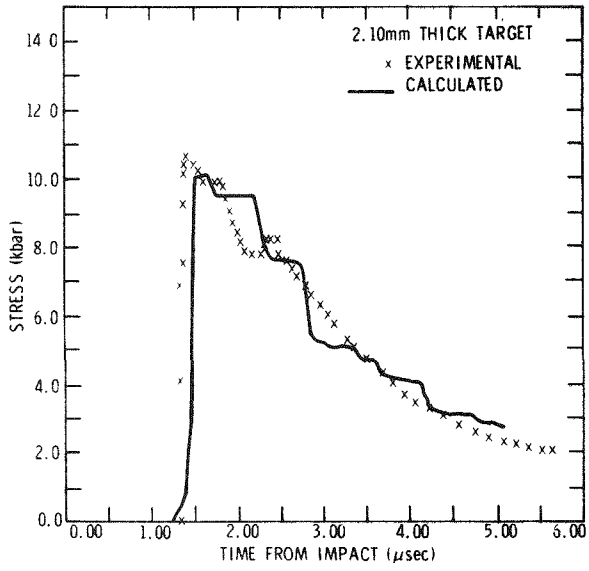

14(b)

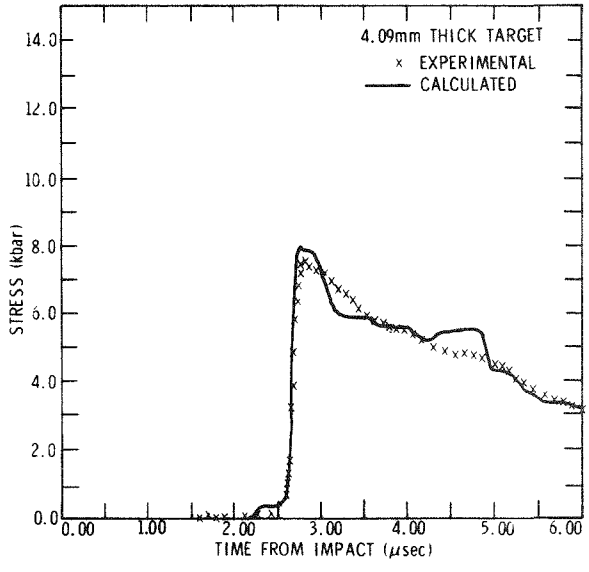

14(c)

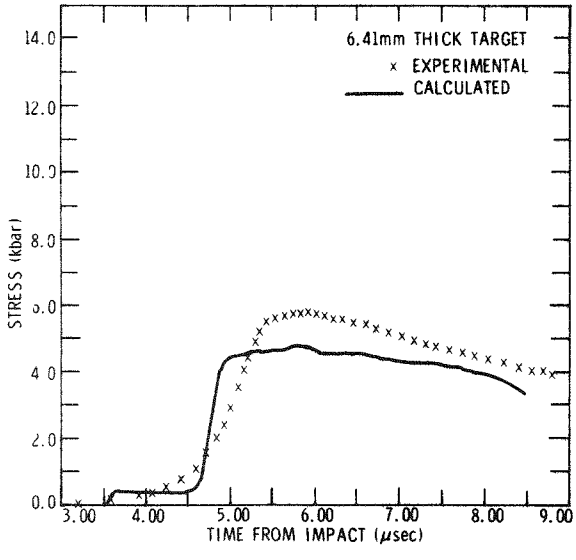

14(d)

FIGURE 14. COMPARISON BETWEEN EXPERIMENTAL AND CALCULATED ATTENUATED WAVE PROFILES FOR CVD CARBON FELT. EXPERIMENTAL DETAILS LISTED IN TABLE III.

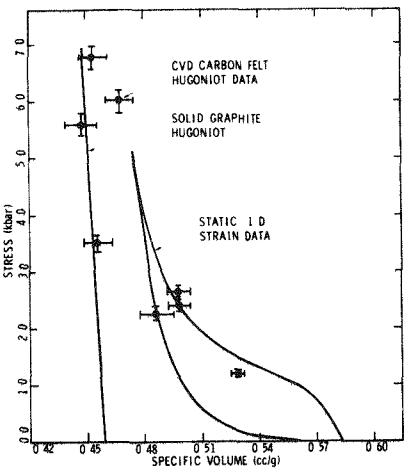

15(a)

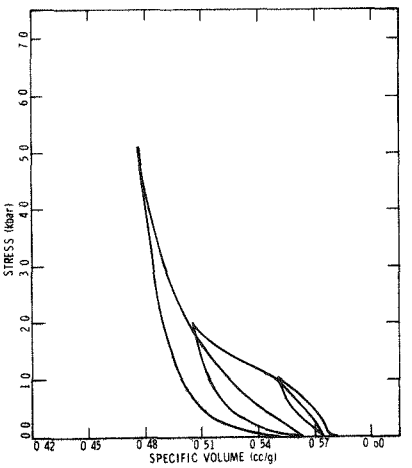

15(b)

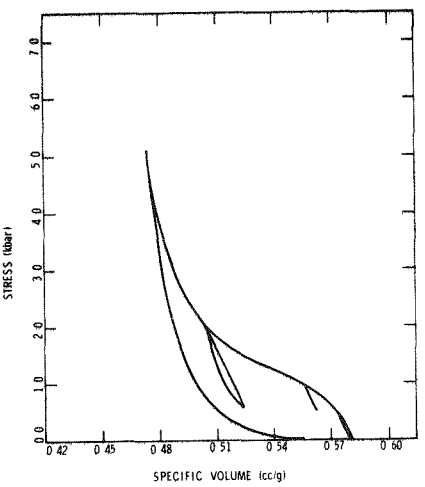

15(c)

FIGURE 15.

STATIC LATERALLY CONSTRAINED STRESS - SPECIFIC VOLUME CURVES FOR CVD CARBON FELT

(a) ONE COMPLETE LOADING CYCLE
(b) THREE COMPLETE LOADING CYCLES
(c) THREE LOADING CYCLES WITH PARTIAL UNLOADING

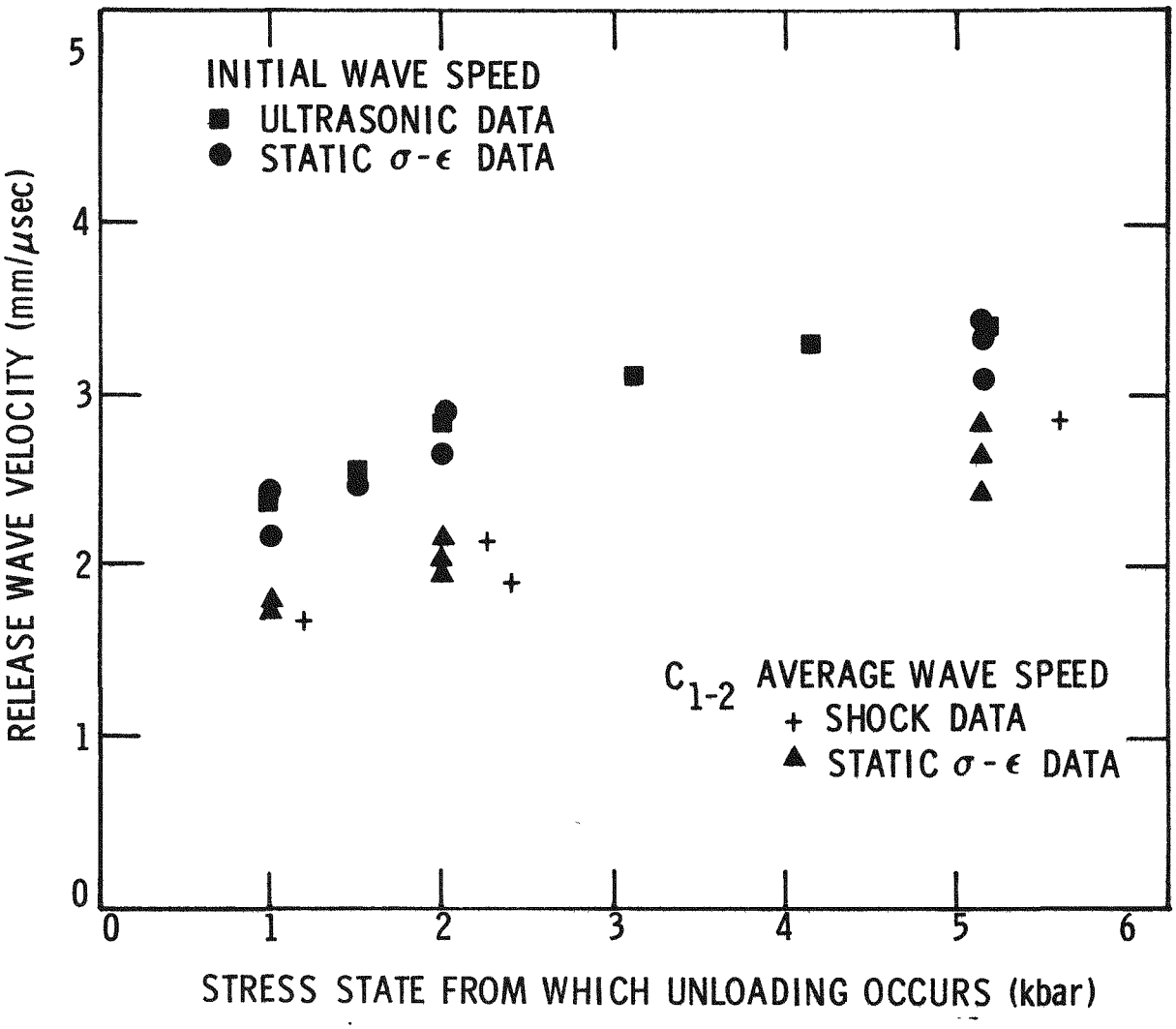

FIGURE 16. COMPARISON OF RELEASE WAVE SPEEDS FROM STATIC AND SHOCK EXPERIMENTS ON CVD CARBON FELT

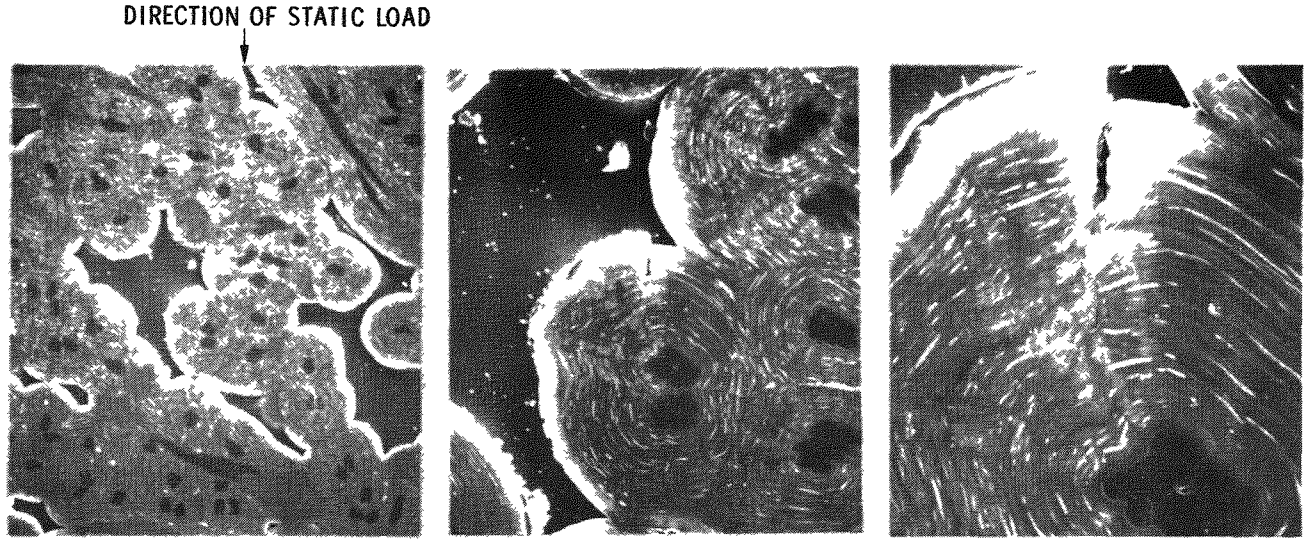

17(a) 0.3 KX

17(b) 1.0 KX

(17(c) 3.0 KX

FIGURE 17. SEM PHOTOMICROGRAPHS OF CVD CARBON FELT MATERIAL DAMAGE RESULTING FROM STATIC COMPRESSION TO 5.1 kbars

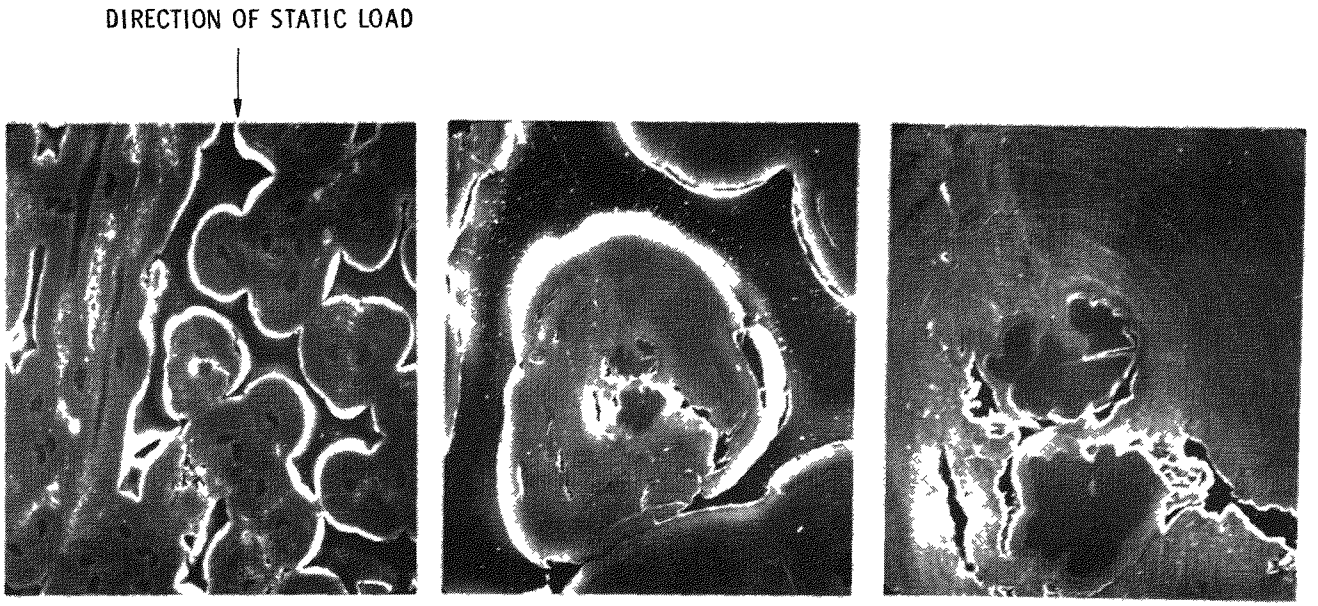

18(a) 0.3 KX 18(b) 1.0 KX 18(c) 3.0 KX

FIGURE 18. SEM PHOTOMICROGRAPHS OF CVD CARBON FELT MATERIAL DAMAGE RESULTING FROM STATIC COMPRESSION TO 5.1 kbars

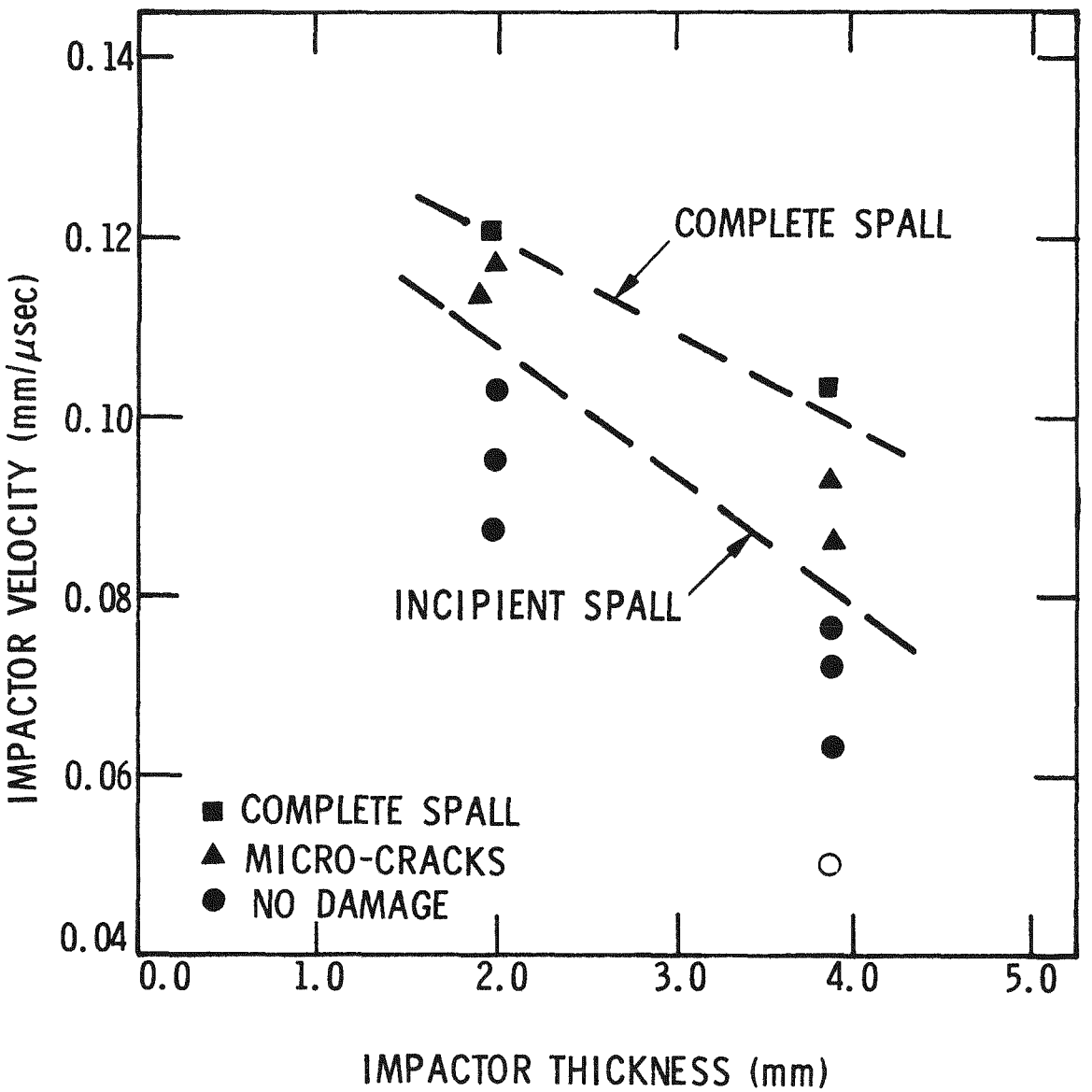

FIGURE 19. SPALLATION DATA FOR CVD CARBON FELT

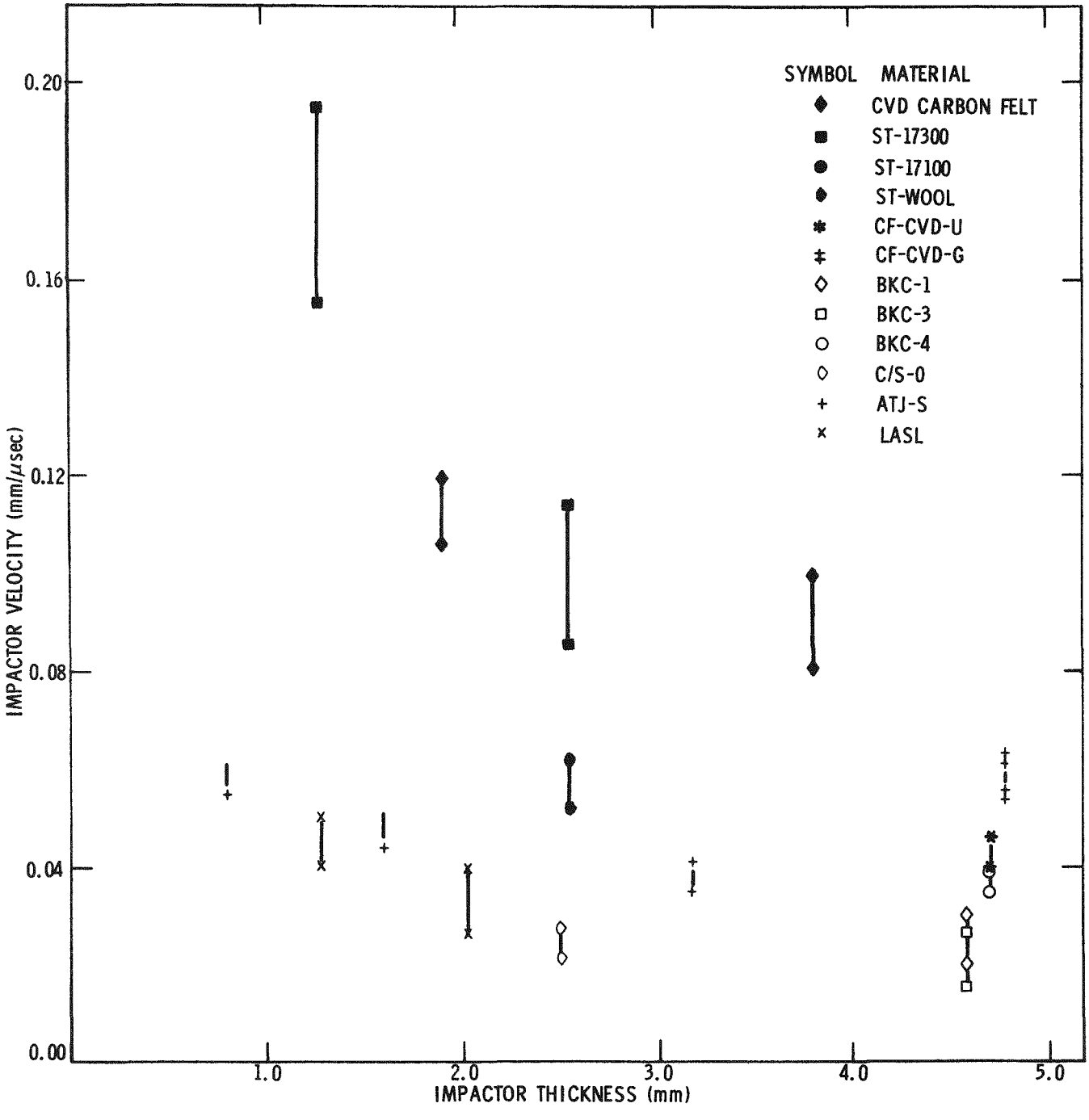

FIGURE 20. POROUS CARBON AND GRAPHITE SPALL DATA. DETAILS IN TABLES V AND VI.

Distribution:

Aerospace Corporation (8)
P. O. Box 92957
Los Angeles, California 90009
Attn: W. J. Barry, Jr.
R. J. Rausch
S. A. Batdorf
R. L. Crolius
S. L. Channon
G. R. Schneiter
R. B. Mortensen
W. E. Schorr

Air Force Institute of Technology
Wright-Patterson AFB
Dayton, Ohio 45433
Attn: P. J. Torvik

Air Force Matls. Lab. (3)
Wright-Patterson AFB
Dayton, Ohio 45433
Attn: N. Pogano LNP
S. Tsai
T. Nicholas

Air Force Weapons Laboratory (8)
Kirtland Air Force Base
Albuquerque, New Mexico 87117
Attn: A. H. Guenther - WLZ
H. Cooper
Col. O. B. Cunningham
Lt. Col. C. Weiss
Lt. Col. D. D. Young
Maj. C. S. Lee
Capt. J. B. Webster
Capt. J. A. Gordon

Army Materials and Mech. Res. Center (4)
Appl. Mech. Research Lab.
Watertown, Mass. 02172
Attn: S. C. Chou
K. H. Abbott
J. Bluhm
J. Dignam

AVCO Corporation (2)
Research and Advanced Dev. Divn.
201 Lowell Street
Wilmington, Mass. 01887
Attn: W. L. Bade
R. E. Cooper

AWRE Distribution (5)
Attn: L. C. Guynes
Organization 1000, Sandia Laboratories
For: B. D. Lamborn
N. E. Hopkin
G. Eden
C. P. M. Smith
J. Martin

Ballistic Research Laboratories (5)
Aberdeen Proving Ground, Maryland 21005
Attn: M. Moss, Director AMXRD-BTL,ARDC
J. T. Frasier
R. Vitali
W. Schuman
Thomas Dolce

Battelle Memorial Institute (3)
505 King Avenue
Columbus, Ohio 43201
Attn: B. D. Trout
M. R. Vanderlind
E. G. Bodine

Bell Telephone Laboratory
Whippany, New Jersey 07981
Attn: N. Beauchamp

The Boeing Company (2)
Aerospace Group
Shock Physics Laboratory
Seattle, Washington 98124
Attn: B. M. Lempriere
J. R. Penning

Brown University
Dept. of Engineering
Providence, Rhode Island 02912
Attn: R. J. Clifton

California Institute of Technoloby
Pasadena, California 91109
Attn: T. J. Ahrens
Dept. of Geophysics
Seismological Lab.

Defense Atomic Support Agency
R & D Officer, Shock Physics
Directorate
Washington, D. C. 20305
Attn: C. B. McFarland

Defense Nuclear Agency (5)
Washington, D. C. 20305
Attn: SPAS, M. C. Atkins
F. S. Celec
R. E. Jackson
D. Kohler
F. Moulton

Drexel University (3)
32nd and Chestnut Streets
Philadelphia, Penn. 19104
Attn: F. K. Tsou
P. C. Chou
S. Gordon

Effects Technology, Inc.
P. O. Box 30400
Santa Barbara, California 93105
Attn: F. R. Tuler

EG&G, Inc.
130 Robinhill Rd.
Goleta, California 93105
Attn: J. Charest

Frankfort Arsenal
Bridge and Tacony Streets
Bldg. 149
Philadelphia, Penn. 18015
Attn: M. Schwartz

General Electric Co. (2)
Valley Forge Space Center
Valley Forge, Pa. 19481
Attn: M. Ben-Amoz
C. H. Mok

Gulf General Atomic
P. O. Box 608
San Diego, Calfornia 92112
Attn: M. J. Nowak

Headquarters, Field Command
Defense Atomic Support Agency
Sandia Base
Albuquerque, New Mexico 87115
Attn: Adjutant General

Kaman Sciences (3)
1700 Garden of the Gods Rd.
Colorado Springs, Colo. 80907
Attn: T. F. Meagher
F. Shelton
D. Williams

Ktech Corp. (2)
Box 5490
Kirtland Air Force Base
Albuquerque, New Mexico 87115
Attn: N. H. Froula
D. Y. Keller

Lockheed Missile and Space Co. (4)
3251 Hanover Street
Palo Alto, California 94304
Attn: A. O. Burford
L. F. Hearne
O. Hoffman
W. E. Jahsman

Massachusetts Inst. of Technology (3)
Aerolastic and Structures Research
Cambridge, Mass. 02138
Attn: E. A. Witmer
T. H. Pian
J. B. Walsh

McDonnell-Douglas Astronautics Co. (2)
Western Division
5301 Bolsa Avenue
Huntington Beach, California 92647
Attn: L. Cohen
J. C. Peck

O. A. Nance
Box 16006
Louisiana State University
Baton Rouge, Louisiana 70803

Commander, Naval Ordnance Lab. (7)
Advanced Chemistry Division
White Oak, Silver Spring, Md. 20910
Attn: W. J. Buehler
John Erkman
L. F. Gowen
T. Harris
M. Huddleston
D. John Pastine
W. Walker

Naval Research Lab.
Washington, D. C. 20390
Attn: J. R. Baker

North Carolina State University
Dept. of Engineering Mechanics
Box 5130
Raleigh, North Carolina 27607
Attn: Y. Horie

Physics International (2)
2700 Merced Street
San Leandro, California 94577
Attn: J. H. Shea
C. Young

Physics International
3151 Fostoria Way
San Ramon, California 94583
Attn: C. F. Cline

Picatinny Arsenal, Bldg. 350 (2)
SMUPA-VC2
Dover, New Jersey 07081
Attn: E. N. Clark
Paul Harris

Southwest Research Institute (3)
8500 Culebra Rd.
San Antonio, Texas 78228
Attn: W. Ko
N. Abramson
E. Lindholm

Stanford University (2)
Division of Engineering Mechanics
Stanford, California 94305
Attn: E. H. Lee
G. Hermann

SAMSO (8)
P. O. Box 9260
Worldwide Postal Center
Los Angeles, California 90009
Attn: Col. A. Aharonian
Lt. Col. K. Gilbert
Capt. Gaylord Green
Capt. James Green
Mr. James Hess
Capt. R. A. Rene
Lt. Col. D. R. Shover
Capt. Tom Swartz

Stanford Research Institute (2)
333 Ravenswood
Menlo Park, California 94025
Attn: D. R. Curran
L. Seaman

Systems, Science and Software (5)
P. O. Box 1620
La Jolla, California 92037
Attn: Russell Duff
R. Kruger
H. E. Read
T. D. Riney
J. M. Walsh

Terra Tek, Inc. (2)
420 Wakara Way
University of Utah Research Park
Salt Lake City, Utah 84108
Attn: S. J. Green
A. H. Jones

TRW Systems (2)
1 Space Park
Redondo Beach, California 90278
Attn: J. Slaughter
R. Mayer

Union Carbide Corp. (3)
Bldg. 9302, Y-12
Oak Ridge, Tenn. 37830
Attn: Clyde M. Davenport
Steven Wallace
J. L. Cook

University of California (14)
Lawrence Livermore Laboratory
P. O. Box 808
Livermore, California
Attn: Reports Library
W. P. Crowley
A. C. Holt
W. B. Isbell
R. N. Keeler
H. W. Kruger
J. J. Ruminar
R. N. Schock
S. Sock
M. van Thiel
R. J. Wasley
M. Wilkins
I. W. Woodruff
J. Lyle

University of California (10)
Los Alamos Scientific Laboratory
P. O. Box 1663
Los Alamos, New Mexico 87544
Attn: Reports Library
Al Davis, J-15
W. Deal, GMX-6
C. L. Mader, T-5
R. G. McQueen, GMX-6
B. P. Shafer, W-1
J. W. Taylor, GMX-11
Rod Thurston, W-4
D. Venable, GMX-11
J. Wackerle, GMX-7

USA Missile Command
Research & Engineering Directorate
Redstone Arsenal, Alabama 35809
Attn: AMSMI-RS W. A. Lewis

USAE Waterways Experiment Station
P. O. Box 631
Vicksburg, Mississippi
Attn: Billy R. Sullivan

U. S. Atomic Energy Commission
Albuquerque Operations Office
P. O. Box 5400
Albuquerque, New Mexico 87115
Attn: H. C. Donnelly

U. S. Atomic Energy Commission
Division of Technical Information
Rep. Sec., Hdqrs. Library, G-017
Washington, D. C. 20545

U. S. Atomic Energy Commission
Sandia Area Office
P. O. Box 5400
Albuquerque, New Mexico 87115

Washington State University (2)
Dept. of Physics
Pullman, Washington 99163
Attn: G. Duval
G. R. Fowles

W. C. Myre, 1210
R. L. Peurifoy, 1220
R. D. Andreas, 1222
J. C. Zimmerman, 1222
S. L. Jeffers, 1223
D. J. Rigali, 1225
J. L. Irwin, 1225
J. J. Marron, 1314
Attn: G. E. Clark
D. M. Olson, 1510
C. H. Mauney, 1530
T. B. Lane, 1540
S. W. Key, 1541
T. G. Priddy, 1542
B. E. Bader, 1543
R. T. Othmer, 1544
D. J. McCloskey, 1715
A. M. Clogston, 5000
A. Narath, 50
O. E. Jones, 5100
F. L. Vook, 5110
G. A. Samara, 5130
L. W. Davison, 5131
B. Morosin, 5132
B. M. Butcher, 5133
L. M. Lee, 5133 (20)
J. E. Schirber, 5150
W. Herrmann, 5160
L. D. Bertholf, 5162
D. E. Munson, 5163
R. P. May, 5163
C. H. Karnes, 5165
J. C. Swearengen II, 5165
A. J. Chabai, 5166
L. W. Kennedy, 5166
L. C. Hebel, 5200
G. W. Gobeli, 5210
J. E. McDonald, 5300
H. M. Stoller, 5310
D. A. Northrop, 5313
B. L. Butler, 5313
B. Granoff, 5313
D. M. Schuster, 5314
T. R. Guess, 5314
A. W. Mullendore, 5315
J. K. Johnstone, 5315
J. D. Theis, 5315
A. W. Snyder, 5320
R. W. Lynch, 5323
R. R. Boade, 5323
C. M. Percival, 5323
K. D. Smith, 5323
L. S. Nelson, 5324
R. T. Meyer, 5324
O. L. Burchett, 5325
W. B. Gauster, 5325
F. C. Perry, 5325

L. M. Berry, 5500
R. G. Kepler, 5510
W. M. O'Neill, 5520
M. J. Davis, 5530
A. Y. Pope, 5600
J. F. Barham, 8130
J. B. Wright, 8131
M. E. Brown, 8131
H. F. Norris Jr., 8131
H. R. Sheppard, 8157
G. E. Brandvold, 8170
A. S. Rivenes, 8175
G. R. Otey, 8178
Library, 8232
R. H. Meinken, 8310
J. H. Brierly, 8311
D. R. Adolphson, 8312
H. J. Saxton, 8312
L. R. Hill, 8314
M. D. Meyer, 8314
G. W. Anderson Jr., 8330
J. L. Wirth, 8340
J. A. Mogford, 8341
E. H. Barsis, 8342
S. G. Cain, 8343
A. N. Blackwell, 8350
C. W. Robinson Jr., 8352
L. M. Murphy, 8352
C. S. Hoyle, 8353
W. D. Zinke, 8414
J. D. Kennedy, 9110
R. C. Bass, 9111
G. W. Barr, 9114
J. W. Wistor, 9116
R. P. Reed, 9116
J. L. Gardner, 3140
A. M. Torneby, 3141 (4)
R. S. Gillespie, 3151 (3)
for AEC/TIC (Public Release)